

RESPONSE TO COMMENTS

Title: UAV-enabled reconnaissance and trajectory modeling of a co-seismic rockfall in Lefkada

Journal: NHESS

We note that the reviewers are positive about our manuscript. We appreciate the time taken by both reviewers to consider the manuscript and agree that their comments have given us constructive ideas on how to improve this contribution.

The manner in which the comments are addressed is given below:

REVIEWER 1:

GENERAL COMMENTS

Comment 1: The title should probably be changed in something like “UAV-based back analysis and trajectory modelling of a co-seismic rockfall in Lefkada”.

Response: We changed the title as follows:

UAV-based mapping, back analysis and trajectory modelling of a co-seismic rockfall in Lefkada Island, Greece”.

Comment 2:

From the manuscript is not clear how the images or videos have been processed nor is the accuracy of the DSM discussed in detail.

Response: Text was added – line 122 to 131. Figure 4 and 5 were added.

We follow the typical procedures for Structure-from-Motion as laid out in the following Figure, which will be added in the manuscript. These include the following steps:

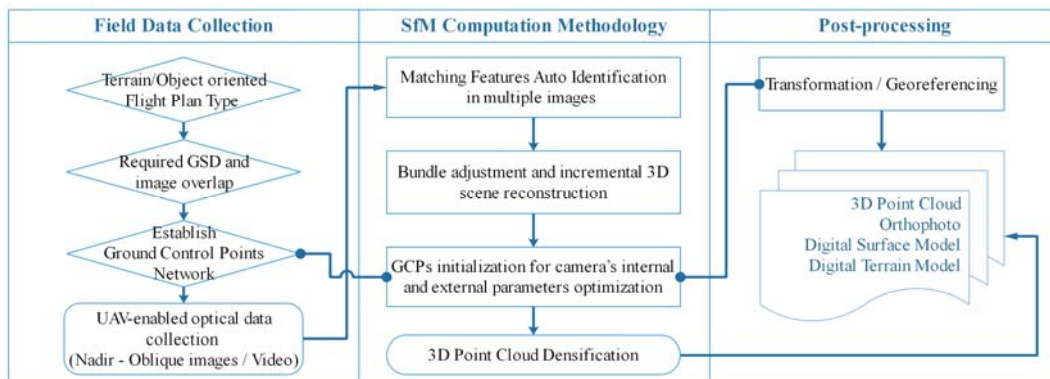
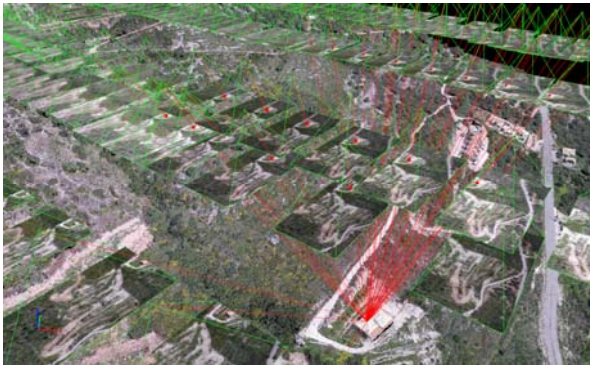


Figure 3

32 In addition, the accuracy of the model has been examined by using portions of the
33 ground control points and developing DEM of differencing between different models,
34 an investigation that is described in our paper by Manousakis et al. (2016). Finally, we
35 have also made a comparison, and we plan to add that in our paper, of the DEM
36 developed by the UAV against the satellite-based DEM that is part of the Greek
37 cadastre. The two surfaces were found to be very similar.

38 The overlap between pictures was minimum frontal 80%, side 65% and a total of 714
39 camera station (video frames extracted) were included (see the following Figure).



40

41 **Figure 4**

42 **Comment 3:**

43 In the 3D simulations it looks like the authors used the DSM that still includes
44 vegetation. This might create unrealistic obstacles.

45

46 **Response: Text was added – line 158 to 182.**

47 The vegetation was removed from the DSM.

48 For vegetation removal, Point Cloud neighbourhood examination and DEM smoothing
49 algorithms have been implemented. Firstly, a bare-Earth digital elevation model (DEM)
50 from the input point cloud LAS file was interpolated, by specifying the grid resolution
51 (2m) and the inter-point slope threshold. The algorithm distinguishes ground points
52 from non-ground points based on the inter-point slope threshold. The interpolation area
53 is divided into grid cells, corresponding to the cells of the output DEM. All of the point
54 cloud points within the circle encompassing each grid cell is then examined as a
55 neighbourhood. All points within a neighbourhood that have an inter-point slope with
56 any other point and is also situated above the corresponding point, is considered to be
57 a non-ground point. An appropriate value for the inter-point slope threshold parameter
58 will depend on the steepness of the terrain, but generally values of 15-35 degrees
59 produce satisfactory results. The elevation assigned to the grid cell is then the nearest
60 ground point elevation (Whitebox GAT help topics).

61 Further processing of the interpolated bare-earth DEM was introduced to improve
62 vegetation and structures removal results by applying a second algorithm to point cloud
63 DEMs which frequently contain numerous off-terrain objects such as buildings, trees
64 and other vegetation, cars, fences and other anthropogenic objects. The algorithm
65 works by finding and removing steep-sided peaks within the DEM. All peaks within a
66 sub-grid, with a dimension of the user-specified Maximum Off-Terrain Object (OTO)
67 Size, in pixels, are identified and removed. Each of the edge cells of the peaks are

68 then examined to see if they have a slope that is less than the user-specified Minimum
69 OTO Edge Slope and a back-filling procedure is used. This ensures that OTOs are
70 distinguished from natural topographic features such as hills (Whitebox GAT help
71 topics).

72 Algorithms executed within Whitebox GAT Geospatial Analysis Tools platform
73 (<http://www.uoguelph.ca/~hydrogeo/Whitebox/index.html>).

74 **Comment 4:** The influence of the slope roughness is not addressed in detail.
75

76 **Response:** In this study, roughness has been fully taken into account (looking on the
77 block's dimension scale) by the accurate cross-section used in the analyses (more
78 than 1500 x-y points were used – approximately 2 points per meter). This comment
79 was added in the manuscript (line 343-345).

80 **Comment 5:** The authors also use inconsistent and uncommon notation.

81 **Response:** notation has been corrected.

82

83 **SPECIFIC COMMENTS**

84 **Par. 3 (UAV)**

85

86 1. UHD 4K is only relevant if you work with videos, for digital images the
87 sensor size and the pixel resolution are most important.

88

89 **Response:** The sensor is a 1/2.3" CMOS (6.47x3.41mm) and the effective
90 pixel resolution is 12.4 MP (4096x2160 pixels). This information was
91 added in line 92 - 94.

92

93 2. In order to produce orthophoto and DSM you need to process the
94 images, the UAV is a tool to capture the images.

95

96 **Response:** Agreed. The process to do this has been
97 described in the "General comment No. 2" and was added
98 in the paper in line 113 to 122.

99

100 3. see previous comments. Also, the Phantom 3 Pro has an integrated
101 camera.

102

103 4. did you really process the video? or did you use full resolution still
104 images? This is not clear, please provide more details. In addition,
105 provide frame rate and/or number of images

106

107 • **Response:** This information is now added in the paper as part of responding
108 to "General comment No. 2" in line 122 to 131

109 5. again, the DSM results from the image processing. Also, specify the
110 software you used

111 **Response:** The software used was Agisoft Photoscan. This was added in line 152.

112 6. have you used the GCPs for georeferencing only or have you used them as
113 well in the bundle adjustment?

114 **Response:** GCPs were used for both georeferencing and solving camera's internal
115 and external parameters. Total RMS error for 6 GCPs is 0.07m while total RMS error
116 for 4 Check Points is 0.20m. Text added in line 184-187.

117 7. How accurate is your DSM model? Provide some details.

118
119 **Response:** This is now discussed as part of the "General comment No. 2" –
120 See line 186.

121 Total RMS error for 6 GCPs is 0.07m while total RMS error for 4 Check Points
122 is 0.20m. When compared to a 5m DEM from Greek National Cadastre with a
123 geometric accuracy of $RMSE_z \leq 2,00m$ and absolute accuracy $\leq 3,92m$ for a
124 confidence level of 95%, a mean difference of 0.77 m and a standard deviation
125 of 1.25 m is observed, which is well into the range of uncertainty of the cadastre
126 model itself.

127
128 8. Also, a DSM generally includes vegetation and does not represent the
129 true ground surface, which is relevant for rockfall analysis. You should
130 probably work with a DTM (digital terrain model) instead of a DSM.
131 However, this is not straightforward with photogrammetry data. Please
132 comment.

133
134 **Response:** A description on this is now added in comment "General
135 Comment No. 3". See line 158 to 182.

136
137 9. line 136 "Note that this resolution is still higher than the resolution of
138 DSM that are used in rockfall analyses"

139
140 not completely true, depends on the scale

141 **Response:** A comment was added, indicating that this resolution is higher than
142 commonly used for slopes of that size. See text in line 156 – 157.

143

144 **par. 5 (rockfall)**

145 1. correct to COR_v

146 the normal (nCOR) and the tangential (tCOR)

147 Please use commonly used notation. Also what is with the rotational energy (see
148 e.g. Volkwein et al. 2011, NHESS)

149 **Response:** The notation used is found in several relevant papers, therefore it is not
150 uncommon. It is a fact though, that no agreement regarding notation is exist between
151 researchers, as various notations exist for the COR (i.e. R_n, nCOR, K_n and others)

152 We have used a lumped-mass method in our analysis. "Lumped-mass methods
153 consider the block to have either no mass or a mass concentrated into one point and
154 do not take into account either the shape of the blocks or rotational movement"
155 (Volkwein et al. 2011)

156 2. no impacts on trees were recorded, right?

157 **Response:** No impact on trees was recorded. This was added in the manuscript in line
158 279.

159 3. use $1/\cos^2$

160 **Response:** We agree. All equations have been written again

161 4. you should also look in Volkwein et al. (2011 NHSS) as they summarize
162 characteristic jump heights. How do your jump heights compare to those
163 mentioned in the reference?

164 **Response:** The f/s ratio of the jumps are relatively high, more than $1/6$ which
165 characterizes the high jump. The maximum f/s ratio is $\sim 1/3$.

166 Text added in line 379 to 382:

167 “Finally, the bounce height of some impacts seems unrealistically high. For example,
168 the 2nd bounce presents a jump height (f) of ~ 17.5 m over a length (s) of ~ 50 m, resulting
169 to a f/s ratio of $\sim 1/3$, when the characteristic f/s ratios for high, normal and shallow
170 jumps is $1/6$, $1/8$ and $1/12$ respectively, as suggested by Volkwein et al. (2011)”.

171 **5. Par. 5.4 coefficients of restitution**

172

173 I cannot fully agree to this. The block starts by rolling along the slope, it
174 should hence have a considerable rotational velocity. Your calculations
175 however neglect the rotational energy. There is room for improvement
176 here.

177

178 **Response:** As previously mentioned, rotational energy was neglected because of the
179 selection of the lump-mass model for the analysis.

180 Also, it is shown in the literature, that high values of restitution coefficients
181 can be related to the influence of the rotational velocity, low impact angles,
182 block shape etc. (see e.g. Buzzi et al. 2012). This should be discussed in
183 more detail.

184

185 **Response:** A more detailed discussion was added in this section and was enriched
186 with more references (Buzzi et al., 2012, Spadari et al. 2011, Ferrari et al. 2013).

187 Text added in line 327 to 333:

188 “Moreover, normal COR values higher than one were calculated in 11 out of the 15
189 remaining impacts. Normal COR higher than one have been observed in both
190 experimental (e.g. Spadari et al., 2011; Buzzi et al., 2012; Asteriou et al., 2012) and
191 back-analysis studies (e.g. Paronuzzi, 2009) and are connected to irregular block
192 shape and slope roughness, as well as to shallow impact angle and angular motion. A
193 more detailed presentation of the reasons why normal COR exceeds unity can be
194 found in Ferrari et al. (2013).”

195 **References added:**

- 196 • Buzzi O, Giacomini A, Spadari M (2012) Laboratory investigation on high
197 values of restitution coefficients Rock Mechanics and Rock Engineering 45:35-
198 43

- 199 • Ferrari F, Giani GP, Apuani T (2013) Why can rockfall normal restitution
200 coefficient be higher than one? Rendiconti Online Societa Geologica Italiana
201 24.
- 202 • Spadari M, Giacomini A., Buzzi O., Fityus S., Giani G.P. (2011). In situ rockfall
203 testing in New South Wales, Australia. *Int J Rock Mech Mining Sci*, 49, pp. 84–
204 93.
- 205 • Volkwein, A., Schellenberg, K., Labiouse, V., Agliardi, F., Berger, F., Bourrier,
206 F., Dorren, L. K. A., Gerber, W., and Jaboyedoff, M. (2011). Rockfall
207 characterisation and structural protection – a review, *Nat. Hazards Earth Syst.*
208 *Sci.*, 11, 2617–2651, doi:10.5194/nhess-11-2617-2011.

209

- 210 6. The values in the literature vary and calibration of these values with
211 back analysis is generally suggested. Your back analysis suggests a
212 value of n_COR close to 1.

213

214 **Response:** Indeed. This observation is perfectly in-line with those of Buzzi, Giacomini,
215 Wyllie, Asteriou and others. Low impact angle, block's configuration at impact (slope
216 roughness and block's shape) and, maybe, angular velocity lead to n_COR values
217 close to one or even higher. Yet, in the lump-mass model approach, that is the most
218 popular in current practice, those parameters are not taken into consideration.

219

220 Also, what about the slope roughness? It is well known that it has a major
221 influence on the block trajectory.

222 **Response:** Text added in 343 to 348

223 According to Asteriou & Tsiambaos (2016) the most important influence is posed by
224 the impact configuration, which is influenced by slope roughness and block shape. In
225 this study, roughness has been fully taken into account (looking on the block's
226 dimension scale) by the accurate cross-section used in the analyses (more than 1500
227 x-y points were used – approximately 2 points per meter).

228 Based on our knowledge, this accuracy is significantly higher compared to other similar
229 research projects.

230 Moreover, with the data on hand and the lump-mass model analysis we performed, we
231 were not able to simulate block shape effect nor the configuration of the block at
232 impact.

233 7. "friction angle was set to zero"

234

235 Doesn't this imply that the rock is sliding instead of rolling? How did you
236 create your 2D slope profile? What about slope roughness?

237

238 **Response:** According to Rocfall software code (Rocscience Ltd) when friction
239 angle is set to zero the motion of the falling block is rolling.

240

241 In the 2D analysis, the roughness of the slope was intentionally set to zero, as
242 the analysis was deterministic. We didn't consider a standard deviation for

243 the coefficients of restitution, the friction angle and roughness of the material
244 on the slope (text added in line 357 – 359).
245
246 8. Line 310 “Finally, the bounce height of some impacts seems
247 unrealistically high”
248 maybe you can also compare these to the once you back calculated
249
250 **Response:** See reply to earlier comment discussing jump heights. Text added
251 in manuscript in line 379 to 382.
252
253 **9. par. 3D rockfall analysis**
254 You address slope roughness here but not in your 2D simulations.
255
256 **Response:** Text added in line 394 – 397
257
258 “The slope roughness was modeled using the mean obstacle height (MOH),
259 which is the typical height of an obstacle that the falling block encounters on
260 the slope at a possibility percentage of 70%, 20% and 10% (rg10, rg20, rg70)
261 of the trajectories (according to the suggested procedure in Rockyfor3D)”.
262 As mentioned earlier, the slope roughness was not taken into account in the 2D
263 analysis as the slope terrain was produced with much great accuracy.
264
265 10. Line 393 “estimation of the initial velocity of the blocks plays a
266 significant role in the accurate re-production of the rockfall trajectory.”
267
268 Did you do a sensitivity study on the initial velocity in order to conclude
269 this?
270 **Response:** Yes, a sensitivity study was performed using a range of values for the
271 initial velocity.
272
273 **11. Table 3**
274 use same notation as in the text
275 **Response:** Corrected
276
277 **12. Figure 3**
278 number all impacts
279
280 **Response:**
281 All impacts are numbered in Figure 6, where it is important to compare the
282 actual trajectory with the rockfall analysis. Figure 3 shows the actual trajectory
283 and we believe it is not necessary to number all the impacts on this figure.
284
285 use consistent numbers, change the numbers according to the number of
286 impact as also shown in Fig. 6
287 **Response:** See previous comment
288
289 is the block rolling from the detachment point until the first impact
290 **Response:** The block is rolling from the detachment point until the first impact,
291 as clearly stated in par. 3.2.
292
293 **13. Figure 13**

293 It is interesting to note that a very strong dispersion starts right at the source. Do you
294 have a clear explanation for this? Also, the vegetation might play an important role
295 during the rolling phase. Is the rolling phase more realistic in these simulations
296 compared to the one of Rocfall? How many simulations did you perform? Could you
297 perform more simulations? Finally, it seems that the DSM includes a lot of vegetation
298 but you also model roughness by MOH although you say no vegetation was considered
299 in the analysis (line 323-327). This is kind of contradicting and needs to be clarified

300

301 **Response:** Text added in line 432 - 433

302 It is true that there is a strong dispersion at the source. The reason for this dispersion
303 is the topography effect of the area of detachment, as discussed in par. 6.3.

304 We performed a significant number of simulations (with a range of restitution
305 parameters. The scope was to run the 3D analysis according to the restitution
306 parameters and soil types suggested by Rockyfor3D and discuss the results. The total
307 number of simulated falling rocks (total nr. of simulations) was 120 for each analysis.

308 As explain in the response of a previous comment, the vegetation was removed from
309 the DSM. The roughness, which was considered in the 3D analysis, refers to the slope
310 terrain (not the vegetation) and is modelled according to the suggested method of
311 Rockyfor3D using coefficients rg10, rg20, rg70 (see previous comment).

312

REVIEWER 2:

313

314 **Comment 1**

315 How many days after earthquake was made the UAV acquisition

316 **Response:** Text added in line 95 – 97.

317 There was an immediate UAV acquisition that was conducted 2 days after the
318 earthquake. A second more detailed UAV acquisition with the objective to create a
319 DEM was made 5 months after the rockfall event.

320 **Comment 2**

321 In the figure 1 may useful to have map that localize study area inside Greece, and also
322 to add a scale bar to figure

323 **Response:** We added a new Figure (Figure 1) to localize the study area in Greece

324 **Comment 3**

325 In figure 3 is better to put the impact point photo in the same orientation of the track.

326 Text was also added in line 76 – 80.

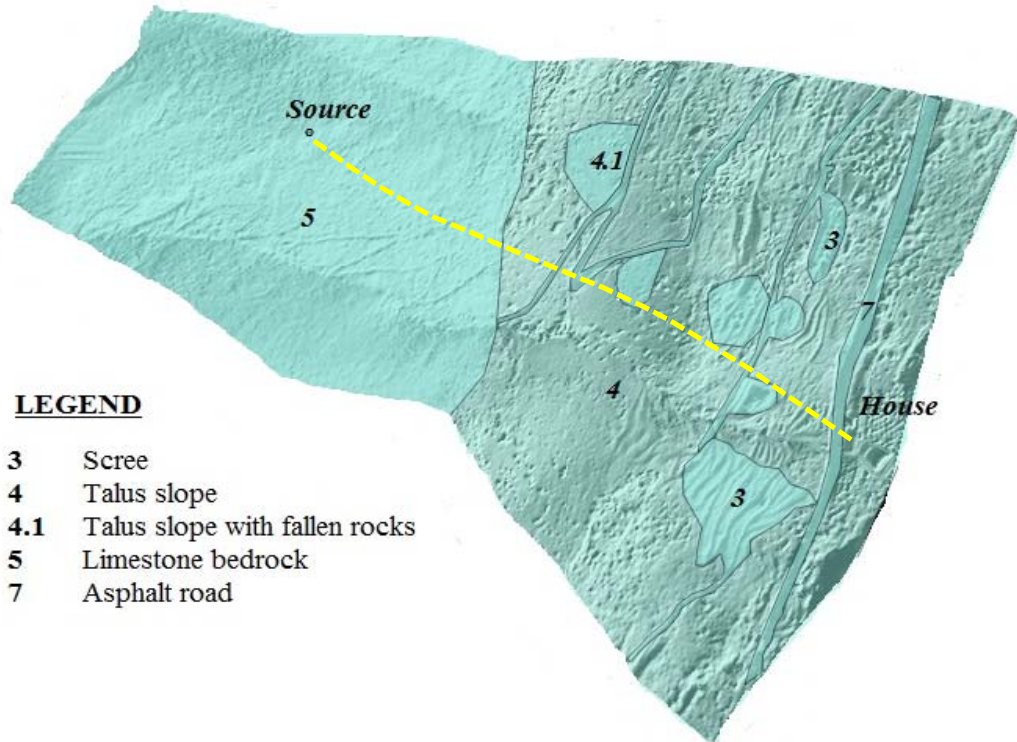
327 **Response:** We rotated the figure (see below).



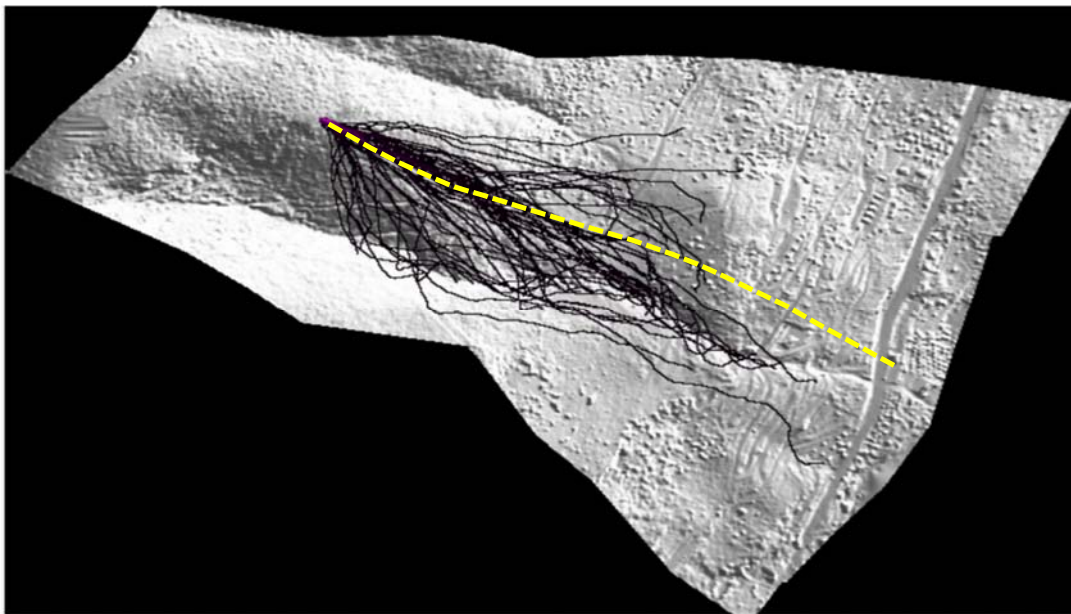
328

329 **Comment 4**

330 Figure 11 / Figure 13 it will be nice add the real path of rockfall for comparison
331 with
332 the results from simulations.
333 **Response:** We added the actual path on the Figures.



334
335 Figure 11



336
337 Figure 13
338 **Comment 5**

339 Revise to find and correct some typo errors like: > Line 113: the > the > Line
340 114 onhore > onshore ?

341 **Response:** Corrected

342 **Comment 6**

343 reference: check that all references are in the format required by NHESS Smith,
344 P.,
345 Thomson, A., and Carter, T.:, 2006.

346 **Response:** Corrected

347

348

349 **THIS VERSION OF THE MANUSCRIPT SHOWS THE MAJORITY**
350 **(BUT NOT ALL) OF CHANGES (USING EITHER RED INK OR TRACK**
351 **CHANGES THAT WERE MADE AMONG CO-AUTHORS IN REVISING**
352 **THIS MANUSCRIPT. A CLEAN COPY IS ALSO SUBMITTED.**

353 **UAV-based mapping, back analysis and trajectory modelling of a**
354 **co-seismic rockfall in Lefkada Island, Greece**

356
357 Charalampos Saroglou^{1*},

358 Pavlos Asteriou¹

359 Dimitrios Zekkos²

360 George Tsiambaos¹

361 Marin Clark³

362 John Manousakis⁴

363 ¹Department of Geotechnical Engineering, School of Civil Engineering, National Technical
364 University of Athens

365 ²Department of Civil and Environmental Engineering, University of Michigan, USA

366 ³Department of Earth and Environmental Science, University of Michigan, USA

367 ⁴Elxis Group, S.A, Athens, Greece

368 * corresponding author: saroglou@central.ntua.gr

369
370
371 **Abstract**

372 ~~The paper~~We presents ~~the~~ field evidence and ~~the~~ kinematical study of ~~rock block the~~
373 motion ~~of a rock block~~ mobilised ~~in the Ponti area~~ by ~~an~~ ~~M_w 6.5~~ earthquake ~~induced~~
374 ~~rockfall near the island of in the Ponti area of in the island of~~ Lefkada ~~island during a~~
375 ~~M_w 6.5 earthquake~~ on 17th November 2015. A detailed ~~field~~ survey was
376 ~~conducted~~ ~~deployed~~ using an Unmanned Aerial Vehicle (UAV) with an ultra-high
377 definition (UHD) camera, which produced a high-resolution orthophoto and a Digital
378 Surface Model (DSM) of the terrain. The sequence of impact marks from the rock
379 trajectory on the ground surface was identified ~~using from~~ the orthophoto and ~~field~~
380 verified. ~~through a detailed field survey.~~ Additionally, ~~the calculation of~~ earthquake

381 characteristics ~~were determined in order to~~ defined the acceleration ~~on of~~ the rock
382 slope and the initial conditions of the detached block. Using the impact points from the
383 ~~actual measured~~ rockfall trajectory, an analytical ~~reconstruction of the trajectory was~~
384 ~~developed approach to reconstruct the trajectory was implemented~~, which led to some
385 insights on the coefficients of restitution. ~~In order to match the~~ ~~actual measured~~
386 trajectory ~~was compared with modeled rockfall trajectories using typical recommended~~
387 ~~parameters, 2D and 3D rockfall analyses were performed using the recommended set~~
388 ~~of parameters~~. However, the actual trajectory could not be accurately predicted,
389 revealing limitations of existing models.

390 **Keywords**

391 Rockfall, earthquake, DEM, modelling, restitution, UAV

392 **1. Introduction**

393 Active faulting, rock fracturing and high rates of seismicity contribute to common
394 rockfall hazards in Greece. Rockfalls primarily damage roadways and houses
395 (Saroglou, 2013) and are most often triggered by rainfall and secondly seismic loading.
396 Additionally in recent years, some rockfalls have impacted archaeological sites
397 (Marinos & Tsiambaos, 2002, Saroglou et al., 2012). The Ionian Islands, which
398 includes Lefkada Island, experience frequent M_w 5-6.5 earthquakes, as well as less
399 frequent larger (up to 7.5) earthquakes. The historical seismological record is
400 particularly well constrained with reliable detailed information for at least 23 ~~such~~
401 ~~earthquake~~ events since 1612 ~~that, which~~ induced ground failures at the island of
402 Lefkada. ~~On average, Lefkada experiences a and an average of a~~ damaging
403 earthquake every 18 years. In the recent past, a M_w 6.2 earthquake occurred on August
404 14 2003 ~~and was located~~ offshore the NW coast of Lefkada, ~~and which caused~~
405 ~~landslides, rockslides and rockfalls occurred along the western coast of the island~~
406 ~~(Karakostas et al. 2004, Papathanasiou et al., 2012).~~

407 Significant damage was reported, particularly in the town of Lefkada, where a PGA
408 of 0.42g was recorded. ~~Landslides, rockslides and rockfalls occurred along the western~~
409 ~~coast of the island (Karakostas et al., 2004, Papathanasiou et al., 2012).~~

410 On November 17th 2015, an M_w 6.5 earthquake [again](#) struck the island of Lefkada and
411 triggered a number of landslides, rockfalls and some structural damage. The most
412 affected area by large rockslides was the [western](#) coast of the island, especially along
413 its central and south portion, which are popular [summer](#) tourist destinations (Zekkos
414 et al., 2017). The [coseismic](#) landslides completely covered the majority of the west
415 coast beaches and damaged access roads.

416 [On the southeast side of Lefkada near the Gulf of Vassiliki, a seismically-triggered A](#)
417 [rockfall in Ponti village, which lies in the southeast side of Lefkada near the Gulf of](#)
418 [Vassiliki, was triggered during this earthquake and](#) was responsible for one of two
419 deaths caused by the earthquake (Figure 1). Of particular interest, is the very long
420 travel path of the rock block, which was about 800 m in plan view from the point of
421 detachment to the end of its path. Near the end of the rock fall path, the block impacted
422 a family residence, penetrated two brick walls and killed a person in the house. The
423 block exited through the back of the house and came to rest in the property's backyard.

424 The Ponti village rockfall site is characteristic of earthquake induced rockfall and an
425 example of how seismically-induced rockfall impacts human activities. It also [provides](#)
426 [an opportunity to evaluate 2D and 3D rockfall analysis to predict details of the rockfall](#)
427 [trajectory, based on exemplifies the limitations of common 2D rockfall analysis to predict](#)
428 [specific aspects of the rockfall trajectory as](#) measured by field evidence. In order to
429 create a highly accurate model of the rockfall propagation in 2D and 3D space, the
430 rock path and the impact point on the slope was identified by a field survey. The study
431 was performed using an Unmanned Aerial Vehicle (UAV) with an ultra-high definition
432 (UHD) camera, which produced a high-resolution orthophoto and a Digital Surface
433 Model (DSM) of the terrain. The orthophoto was used to identify the rolling section and

434 the bouncing points of the rock along its trajectory, which were verified by field
435 observation. The high-resolution DSM made it possible to ~~conduct~~perform kinematical
436 rebound analysis and a 3D rockfall analysis.

437 **2. Ponti rockfall - site conditions**

438 The locations of the epicenters of the 2003 and 2015 events, as well as the location of
439 the rockfall study site are shown in Figure 1. The southwest coast of Lefkada is part of
440 the Triassic to Eocene age Paxos zone and consists of limestones and dolomites that
441 are covered by Neogene clastic sedimentary rocks, mostly sandstones and marls.
442 Figure 1 also shows faults and high rockfall hazard areas as identified by Rondoyanni
443 et al. (2007). The rockfall at Ponti is not located in a high, as shown on the neotectonic
444 map in Figure 1 (Rondoyanni et al., 2012). ~~The locations of the epicenters of the 2003~~
445 ~~and 2015 events, as well as the location of the rockfall study site are shown in Figure~~
446 ~~1~~ rockfall hazard area. Based on measurements conducted at one location along the
447 rockfall path using the Multichannel Analysis of Surface Waves method, the in-situ
448 shear wave velocity of the top layer was estimated to be around 800 m/sec, which is a
449 high velocity and consistent with the rock conditions expected at the site.

450 The slope overhanging Ponti village is ~~formed in~~made of limestone and has a
451 maximum height of 600 m and an average slope angle of 35° to 40° (Figure 2). The
452 geological formations at the Ponti rockfall site are limestones covered by moderately
453 cemented talus materials. The thickness of the talus materials ranges between 0.5 and
454 4.0 to 5.0 m. A few fallen limestone blocks were identified on the scree slope, with
455 volumes between 0.5 and 2 m³. Based on the size distribution of these rocks on the
456 slope, the average expected block volume would be in the order of 1 to 2 m³.

457 The rockfall release area was at an elevation of 500 m, while the impacted house at
458 an elevation of 130 m (Figure 3). The volume of the detached limestone block was
459 approximately 2 m³ and its dimensions equal to 1.4 m x 1.4 m x 1 m. There was no

460 previous rockfall incident reported for the specific slope that impacted the road or
461 house.

462 3. UAV mapping

463 3.1. Introduction

464 ~~An immediate UAV acquisition that was conducted 2 days after the earthquake. A~~
465 ~~second more detailed UAV acquisition with the objective to create a DEM was made 5~~
466 ~~months after the rockfall event.~~

467 A quadrotor UAV (Phantom 3 professional) was deployed to reach the uphill terrain
468 that was practically inaccessible. The UAV ~~was~~ equipped with an Ultra-high
469 definition (UHD) 12 MP camera and ~~had~~s the capacity to collect 4K video. ~~The sensor~~
470 ~~was a 1/2.3" CMOS (6.47x3.41mm) and the effective pixel resolution was 12.4 MP~~
471 ~~(4096x2160 pixels). An immediate UAV data acquisition expedition that was~~
472 ~~conducted 2 days after the earthquake. A second more detailed mapping UAV~~
473 ~~expedition acquisition with the objective to create a DEM was conducted~~
474 ~~made 5~~
475 ~~months after the rockfall event.~~

476 The first objective of the UAV deployment was to find the initiation point of the rock
477 and then identify the rockfall path (shown in Figure 2). A particular focus on that part
478 of the task was the identification of rolling and bouncing sections of the rockfall path.
479 In addition, in order to generate a high-resolution orthophoto of the rockfall trajectory,
480 aerial video imagery was collected, and the resulting digital surface model (DSM) was
481 used to perform rockfall analysis.

482 ~~The~~ Structure-from-Motion (SfM) methodologies ~~was~~ implemented to create a 3D
483 point cloud of the terrain and develop a 3D model. ~~The methodology is based on~~ ~~by~~
484 identifying matching features in multiple images, ~~and thus imagery overlap of at least~~
485 ~~70% is required.~~ Compared to classic photogrammetry methodologies, where the

486 location of the observing point is well established, SfM tracks specific discernible
487 features in multiple images, and through non-linear least-squares minimisation
488 (Westoby et al., 2012), iteratively estimates both camera positions, as well as object
489 coordinates in an arbitrary 3D coordinate system. In this process, sparse bundle
490 adjustment (Snavely et al., 2008) is implemented to transform measured image
491 coordinates to three dimensional points of the area of interest. The outcome of this
492 process is a sparse 3D point cloud in the same local 3D coordinate system (Micheletti
493 et al., 2015). Subsequently, through an incremental 3D scene reconstruction, the 3D
494 point cloud is densified. Paired with GPS measurements of a number of control points
495 (~~in this case~~ for this site, 10 fast-static GPS points were collected) at the top, middle
496 and bottom of the surveyed area, the 3D ~~model~~ point cloud is georeferenced to a
497 specific coordinate system and through post-processing a digital surface model (DSM)
498 or digital terrain model (DTM) and orthophotos are created. The SfM methodology
499 was implemented in this study using the Agisoft Photoscan software.

500 ~~The typical procedures for Structure-from-Motion were used in the present study,~~
501 ~~following the workflow described in Figure 4.~~

502 In addition, the accuracy of the model has been examined by using portions of the
503 ground control points and developing DEM of differencing between different models,
504 an investigation that is described in our paper by Manousakis et al. (2016). Finally, a
505 comparison was made of the DEM developed by the UAV against the satellite-based
506 DEM that is part of the Greek cadastre. The two surfaces were found to be very similar.

507 The overlap between pictures was minimum frontal 80%, side 65% and a total of 714
508 camera station (video frames extracted) were included as shown in Figure 54.

509 **3.2. High-resolution Orthophoto**

510 A 5cm pixel size orthophoto was generated based on the methodology outlined
511 earlier. As shown in Figure 65, the rolling section and the bouncing locations of the

512 rock block throughout its course were identified. The rolling section ~~was~~ discerned as
513 a continuous and largely linear mark left in the densely vegetated terrain that ~~was~~
514 indicative of the damage caused. Impact points that are part of the bouncing section
515 of the rock, ~~we~~ are identified as circular to ellipsoidal bare earth craters with no
516 disturbance in between. The last bouncing point before impacting the house is clearly
517 identified on the paved road. The plan view ortho-imagery, along with the original
518 footage of the video collected was crucial to the qualitative identification of these
519 features. The alternative, i.e., land-based, conventional field reconnaissance was
520 ~~practically-physically~~ impossible to perform in the ~~the~~ densely vegetated and steep
521 terrain.

522 3.3. Digital Surface Model

523 A profile section and a 10 cm Digital Surface Model (DSM) paired with the plan view
524 orthophoto were first developed (Manousakis et al., 2016) allowing the identification of
525 terrain features such as structures, slope benches or high trees, ~~that which~~ could affect
526 the rock's path downhill. However, this resolution of the DSM proved to be not only
527 unnecessarily high and thus difficult to manipulate in subsequent rockfall analyses, but
528 also resulted in numerical instabilities during the rockfall analyses. Therefore, a
529 downscaled 2 m DSM was produced for the rockfall analysis, ~~using Agisoft Photoscan~~
530 ~~software~~. This was implemented through an aggregate generalization scheme where
531 each output cell is assigned the minimum of the input cells that are encompassed by
532 that cell. In addition, noise filtering and smoothing processing were implemented to
533 reduce the effect of construction elements and vegetation in the final rasterized model.

534 ~~Note that this resolution is still higher than the resolution of DSM that are often used in~~
535 ~~rockfall analyses.~~

536

537 Algorithms for vegetation removal were executed within Whitebox GAT Geospatial
538 Analysis Tools platform. GCPs were used for both georeferencing and solving
539 camera's internal and external parameters. The process involves

540 Point Cloud neighbourhood examination and DEM smoothing algorithms ~~have been~~
541 ~~implemented for vegetation removal.~~ Firstly, a bare-Earth digital elevation model
542 (DEM) was interpolated from the input point cloud LAS file, by specifying the grid
543 resolution (2m) and the inter-point slope threshold. The algorithm distinguished ground
544 points from non-ground points based on the inter-point slope threshold. The
545 interpolation area was divided into grid cells, corresponding to the cells of the output
546 DEM. All of the point cloud points within the circle encompassing each grid cell were
547 then examined as a neighbourhood. All points within a neighbourhood that have an
548 inter-point slope with any other point and are also situated above the corresponding
549 point, are considered to be a non-ground point. An appropriate value for the inter-point
550 slope threshold parameter depends on the steepness of the terrain, but generally
551 values of 15-35 degrees produce satisfactory results. The elevation assigned to the
552 grid cell was then the nearest ground point elevation (Whitebox GAT help topics).

553 Further processing of the interpolated bare-earth DEM was introduced to improve
554 vegetation and structures removal results by applying a second algorithm to point cloud
555 DEMs, which frequently contain numerous off-terrain objects such as buildings, trees
556 and other vegetation, cars, fences and other anthropogenic objects. The algorithm
557 works by finding and removing steep-sided peaks within the DEM. All peaks within a
558 sub-grid, with a dimension of the user-specified Maximum Off-Terrain Object (OTO)
559 Size, in pixels, were identified and removed. Each of the edge cells of the peaks were
560 then examined to see if they had a slope that is less than the user-specified Minimum
561 OTO Edge Slope and a back-filling procedure was used. This ensured that OTOs are
562 distinguished from natural topographic features such as hills (Whitebox GAT help
563 topics).

564 ~~Algorithms were executed within Whitebox GAT Geospatial Analysis Tools platform.~~
565 ~~GCPs were used for both georeferencing and solving camera's internal and external~~
566 ~~parameters.~~

567 Total RMS error after filtering for 6 GCPs was 0.07m, while total RMS error for 4 Check
568 Points was 0.20m. When compared to a 5m DEM from Greek National Cadastre with
569 a geometric accuracy of $RMSE_z \leq 2,00m$ and absolute accuracy $\leq 3,92m$ for a
570 confidence level of 95%, a mean difference of 0.77 m and a standard deviation of 1.25
571 m is observed, which is well into the range of uncertainty of the cadastre model itself.

572 **4. Earthquake characteristics – Initial conditions**

573 **4.1. Seismic acceleration**

574 The epicenter of the earthquake according to the National Observatory of Athens,
575 Institute of Geodynamics (NOA) is located onshore near the west coast of Lefkada.
576 The causative fault is estimated to be a near-vertical strike-slip fault with dextral sense
577 of motion (Ganas et al., 2015, 2016). Based on the focal mechanism study of the
578 earthquake, it was determined that the earthquake was related to the right lateral
579 Kefalonia-Lefkada Transform Fault (KLTF), which runs nearly parallel to the west
580 coasts of both Lefkada and Kefalonia island, in two segments (Papazachos et al. 1998,
581 Rondoyanni et al. 2012). ~~The previous earthquake in this zone occurred in August~~
582 ~~2003 with a magnitude of 6.2.~~

583 A strong motion station recorded the ground motions in the village of Vasiliki located
584 at a distance of 2.5 km from the [Ponti rockfall](#) site. The ground motion characteristics
585 of the recording are summarized in Table 1 and are presented in Figure 76, according
586 to an ITSAK preliminary report (ITSAK, 2016). ~~In comparison with the recordings at~~
587 ~~other locations in Central Ionian, it was evident that the strongest acceleration was~~
588 ~~encountered in Vasiliki area.~~

589 **4.2. Topography effect**

590 Peak ground acceleration along the rock slope is the intensity of base shaking modified
591 by site and topographic effects (Mavrouli et al., 2009). In the present case, local
592 shaking intensity in terms of horizontal PGA was considered. The E-W component of
593 acceleration was considered for the determination of the initial velocity. The peak
594 ground acceleration (PGA) on the slope face (PGA_{sf}) was obtained by linear
595 interpolation between the acceleration at the base (PGA_b) and at the slope crest
596 (PGA_{cr}). The acceleration at the base was equal to 0.32g and thus at the crest $PGA_{cr} =$
597 $1.5 PGA_b$ equal to 0.48g. ~~g. was estimated at the site of detachment. Therefore, the~~
598 ~~seismic acceleration on the slope at the detachment point was calculated equal to 0.45~~
599 ~~g.~~

600 4.3. ~~Assessment~~ Initial velocity of rock block's initial velocity

601 The initial horizontal velocity of the block, at the time of detachment, was calculated
602 considering equilibrium of the produced work and the kinetic energy according to
603 equation 1.

$$604 \quad v_x = \sqrt{2 \times PGA_{sf} \times s} \quad (1),$$

605 where PGA_{sf} is the acceleration on the slope at the location of detachment and s the
606 initial displacement of the block in order to initiate its downslope movement.

607 The initial horizontal velocity was calculated equal to 0.67 m/sec, considering a
608 displacement in the order of $s = 0.05$ m. The vertical component of the initial velocity
609 is assumed to be zero.

610 5. Trajectory analysis

611 In order to estimate the possible rock paths and design remedial measures, simulation
612 programs based on lumped-mass analysis models are commonly used in design
613 practice, ~~which are mostly based on the lumped mass analysis model.~~ The trajectory
614 of a block is modelled as a combination of four motion types; free falling, bouncing,
615 rolling and sliding (Descoedres and Zimmermann, 1987). Usage of the lump-mass

616 model has some key limitations; the block is described as rigid and dimensionless with
617 an idealized shape (sphere); therefore the model neglects the block's actual shape and
618 configuration at impact, even though it is evident that they both affect the resulting
619 motion.

620

621 **5.1. Modelling the response to an impact**

622 The most critical input parameters are the coefficients of restitution (COR), which
623 control the bouncing of the block. In general, the coefficient of restitution (COR) is
624 defined as the decimal fractional value representing the ratio of velocities (or impulses
625 or energies; depending on the definition used) before and after an impact of two
626 colliding entities (or a body and a rigid surface). When in contact with the slope, the
627 block's magnitude of velocity changes according to the COR value. Hence, COR is
628 assumed to be an overall value that takes into account all the characteristics of the
629 impact; including deformation, sliding upon contact point, transformation of rotational
630 moments into translational and vice versa (Giani, 1992).

631 The most widely used definitions originate from the theory of inelastic collision as
632 described by Newtonian mechanics. For an object impacting a rocky slope (Figure-~~8~~
633 ~~7~~), which is considered as a steadfast object, the kinematic COR (v_{COR}) is defined
634 according to Eq. 2.

$$635 \quad v_{COR} = \frac{v_r}{v_i} \quad (2)$$

636 where v is the velocity magnitude and the subscripts i and r denote the trajectory stage;
637 incident (before impact) and rebound (after impact) respectively.

638 Two different mechanisms participate in the energy dissipation process; energy loss
639 normal to the slope is attributed to the deformation of the colliding entities, and in the
640 tangential direction is due to friction between them. Therefore kinematic COR has been

641 analyzed to the normal and tangential component with respect to the slope surface,
642 defining the normal (n_{COR}) and the tangential (t_{COR}) coefficient of restitution (Eq. 3 and
643 4 respectively).

$$644 \quad n_{COR} = \frac{v_{n,r}}{v_{n,i}} \quad (3)$$

645 and

$$646 \quad t_{COR} = \frac{v_{t,r}}{v_{t,i}} \quad (4)$$

647 where the first subscript, n or t denotes the normal or the tangential components of the
648 velocity respectively.

649 Normal and tangential COR have prevailed in natural hazard mitigation design via
650 computer simulation due to their simplicity. Values for the coefficients of restitution are
651 acquired from values recommended in the literature (Azzoni et al. 1995; Heidenreich
652 2004; Richards et al. 2001, RocScience, 2004). Those are mainly related to the surface
653 material type and originate from experience, experimental studies or back analysis of
654 previous rockfall events. This erroneously implies that coefficients of restitution are
655 material constants. However, COR values depend on several parameters that cannot
656 be easily assessed. Moreover, the values suggested by different authors vary
657 considerably and are sometimes contradictory.

658 ~~Usage of the lump-mass model has some key limitations; the block is described as~~
659 ~~rigid and dimensionless with an idealized shape (sphere); therefore the model neglects~~
660 ~~the block's actual shape and configuration at impact, even though it is evident that they~~
661 ~~both affect the resulting motion.~~

662 **5.2. Rockfall path characteristics**

663 23 impact points were identified on the slope surface (Figure 98). Their coordinates
664 are presented in Table 2, along block's path starting from the detachment point (where
665 ~~x=0). No trees were observed along the block's path. impact on trees was recorded.~~

666 The apparent dip of the slope at impact positions was measured from the topographic
667 map; on each impact point a line was set with a length twice the block's mean
668 dimension, oriented according to preceding trajectory direction. Moreover, the impact
669 point was expanded on the topographic map to a rectangular plane with a side twice
670 as much the mean dimension of the block (Figure 94). This plane was then oriented
671 so that one side coincides with the strike direction and its' vertical side toward to the
672 dip direction. Thus, direction difference, $\Delta\phi$, was measured by the strike direction and
673 the preceding path and deviation, e , was measured as the angle between pre and post
674 impact planes (Asteriou & Tsiambaos, 2016).

675 Having a detailed field survey of the trajectory path, a back analysis according to the
676 fundamental kinematic principles was performed in order to back-calculate the actual
677 COR values.

678 **5.3. Kinematic analysis and assumptions**

679 The 23 impact points identified on the slope comprise a rockfall path of 22 parabolic
680 segments. The vertical and horizontal length of each segment is acquired by
681 subtracting consecutive points. Since no external forces act while the block is in the
682 air, each segment lays on a vertical plane and is described by the general equation of
683 motion as:

$$684 \quad y = x \tan \vartheta - \frac{gx^2}{2v_i^2 \cos^2 \vartheta} \quad (5)$$

685 where: θ the launch angle from the horizon and v the launch (initial) velocity (Figure
686 410).

687 Since no evidence can be collected regarding launch angle and velocity, innumerable
688 parabolas satisfy Eq. 5. However, θ is bound between $-\beta$ and 90° , so in order to
689 acquire realistic values for the initial velocity, its sensitivity for that given range was
690 addressed (Figure [4211](#)).

691 For the case presented in Fig. [42-11](#) (the first parabolic segment) it is seen that for the
692 majority of the release angles, initial velocity variation is low and ranges between 7.2
693 and 12 ms^{-1} . Additionally, the relationship between release angle and initial velocity is
694 expressed by a curvilinear function, thus a minimum initial velocity value along with its
695 release angle (denoted hereafter as θ_{cr}) can be easily acquired.

696 Given the minimum initial velocity and the critical release angle for each parabolic
697 segment, the impact velocity and angle can be calculated. Afterwards, normal and
698 tangential velocity components according to the apparent dip of the impact area, are
699 calculated in order to evaluate COR values. Results are summarized in Table 3.

700 **5.4. Coefficients of restitution**

701 It is observed that v_{cor} (Table 3) is slightly greater than one in 5 out of 22 impacts.
702 According to Eq. 3, this can only be achieved when impact velocity is less than rebound
703 velocity. However, this indicates that energy was added to the block during contact,
704 which is not possible according to the law of conservation of energy. Thus, impact
705 velocity should be greater, which is possible if the launch velocity of the previous
706 impact was more than the assumed minimum, ~~as assumed~~.

707 Omitting the impacts with $V_{cor} > 1$, it is observed that kinematic COR ranges between
708 0.55 and 1.0 and presents smaller variation compared to normal or tangential
709 coefficient of restitution, similar to what was previously reported in relevant literature
710 (i.e. Asteriou et al, 2012; Asteriou & Tsiambaos, 2016).

711 The considerably wide scatter of normal COR implies that the restitution coefficient
712 cannot be a material constant. Yet, in most relevant software, normal COR is defined

713 solely by the slope material. Moreover, normal COR values higher than one were
714 calculated in 11 out of the 15 remaining impacts. Normal COR higher than one have
715 been observed in both experimental (e.g. Spadari et al., 2011; Buzzi et al., 2012;
716 Asteriou et al., 2012) and back-analysis studies (e.g. Paronuzzi, 2009) and are
717 ~~connected~~ related to irregular block shape and slope roughness, as well as to shallow
718 impact angle and angular motion. A more detailed presentation of the reasons why
719 normal COR exceeds unity can be found in Ferrari et al. (2013). However, in relevant
720 software normal COR values are bounded between 0 and 1.

721 Moreover, it is observed in Figure ~~13-12~~ that normal COR increases as the impact
722 angle reduces, similarly to previous observations by Giacomini et al. (2012), Asteriou
723 et al. (2012) and Wyllie (2014). The correlation proposed by Wyllie (2014) is also
724 plotted in Figure ~~14-13~~ and seems to describe consistently, but on the unconservative
725 side, the trend and the values acquired by the aforementioned analysis and
726 assumptions.

727 **6. Rockfall modelling**

728 **6.1. 2-D analyses**

729 Initially, a deterministic 2D rockfall analysis was performed using Rocfall software
730 (RocScience, 2004). According to Asteriou & Tsiambaos (2016) the most important
731 influence is posed by the impact configuration, which is influenced by slope roughness
732 and block shape. In this study, roughness has been fully taken into account
733 (~~considering~~ looking on the block's dimension scale) by the accurate cross-section
734 used in the analyses (more than 1500 x-y points were used – approximately 2 points
735 per meter). Based on our ~~knowledge~~ experience, this accuracy is significantly higher
736 compared to other similar research projects. Moreover, with the available data ~~on hand~~
737 and the performed lump-mass model analysis, it was not possible to simulate block
738 shape effect nor the configuration of the block at impact.

739 Considering an initial velocity of 0.67 m/sec, according to the numerical analyses, the
740 falling rock primarily rolls on the slope and stops much earlier than its actual run out
741 distance, approximately 400 m downslope from its starting point (Fig. 98; case 1). The
742 restitution coefficients were $n_{COR}=0.35$, $t_{COR}=0.85$, which represent properties of
743 bedrock outcrops according to the suggested values provided in the documentation of
744 the software.

745 The friction angle was set to zero. A standard deviation for the coefficients of restitution,
746 the friction angle and roughness of the material on the slope was not used, as the
747 analysis was deterministic.

748 If the friction angle is set to $\phi=32^\circ$ (as suggested by the software documentation), the
749 rock travels downslope only 50 m.

750 A separate analysis was performed, with lower coefficients of restitution, resembling
751 that of talus material on the slope ($n_{COR}=0.32$, $t_{COR}=0.82$, $\phi=30^\circ$) as proposed by the
752 suggested values provided in the documentation of the software. In this case, the rock
753 block rolled only a few meters downslope. Therefore, it is evident that the actual rock
754 trajectory cannot be simulated.

755 In order to simulate the actual trajectory as much as possible, various combinations of
756 restitution coefficients and friction angle were considered. The closest match occurred
757 for $n_{COR}=0.60$ and $t_{COR}=0.85$, while the friction angle was set to zero and no velocity
758 scaling was applied. Only in such an analysis, the rock block reaches the house; with
759 a velocity equal to $v=18$ m/s approximately (Fig. 98; case 2). According to the
760 suggested values, these values for the coefficients correspond to a bedrock material
761 (limestone).

762 In this case, the modelled trajectory is significantly different from the actual one. The
763 main difference is that the block is rolling up to 200 m downslope while the actual rolling
764 section is 400 m (as shown in Figure 98). Furthermore the impacts on the ground in

765 the bouncing section of the trajectory are considerably different in number (14 versus
766 23) and in location from the actual ones. Finally, the bounce height of some impacts
767 seems unrealistically high. For example, the 2nd bounce presents a jump height (f) of
768 ~17.5m over a length (s) of ~50m, resulting to a f/s ratio of ~1/3, when the characteristic
769 f/s ratios for high, normal and shallow jumps is 1/6, 1/8 and 1/12 respectively, as
770 suggested by Volkwein et al. (2011).

771 **6.2. 3-D rockfall analysis**

772 The rockfall trajectory model Rockyfor3D (Dorren, 2012) has also been used in order
773 to validate the encountered trajectory and determine the reach probability of the falling
774 rock (from the specific source area) on the impacted house.

775 The 3D analysis was based on the down-scaled 2 m resolution Digital Elevation Model
776 (DEM) that was generated from the 10 cm DSM. The terrain features such as low
777 vegetation (e.g. bushes) and the trees were removed from the DEM as they affected
778 the rock's path downhill. The following raster maps were developed for the 3D analysis:
779 a) rock density of rockfall source, b) height, width, length and shape of block, c) slope
780 surface roughness and d) soil type on the slope, which is directly linked with the normal
781 coefficient of restitution, n_{COR} .

782 The slope roughness was modeled using the mean obstacle height (MOH), which is
783 the typical height of an obstacle that the falling block encounters on the slope at a
784 possibility percentage of 70%, 20% and 10% of the trajectories (according to the
785 suggested procedure in Rockyfor3D). No vegetation was considered in the analysis,
786 which favours a longer trajectory. The parameters considered in the 3D analysis for
787 the different formations are summarised in Table 4. The spatial occurrence of each soil
788 type is shown in Figure 44-13 and the assigned values of n_{COR} are according to the
789 Rockyfor3D manual. The values for soil type 4.1 in Figure 13 are slightly different from
790 soil type 4 (proposed in the manual), denoting talus with a larger percentage of fallen
791 boulders. The block dimensions were considered equal to 2 m³ and the shape of the

792 boulder was rectangle. In order to simulate the initial velocity of the falling rock due to
793 the earthquake, an additional initial fall height is considered in the analysis, which for
794 this case was set equal to 0.5 m.

795 The energy line angles were recalculated from the simulated trajectories and it was
796 determined that the energy line angle with highest frequency (39%) was 30-31°. Based
797 on the 3D analysis no rock blocks would impact the house, although the rock paths are
798 closer to the actual trajectories compared to RocFall software. The reach probability of
799 the falling rocks, initiating from the source point, is shown in Figure 4514.

800 **6.3. Lateral dispersion & Deviation**

801 Lateral dispersion is defined as the ratio between the distance separating the two
802 extreme fall paths (as seen looking at the face of the slope) and the length of the slope
803 (Azzoni and de Freitas 1995). According to Crosta and Agliardi (2004) the factors that
804 control lateral dispersion are classified in three groups: macro-topography factors,
805 factors related to the overall slope geometry; micro-topography factors controlled by
806 the slope local roughness; and dynamic factors, associated with the interaction
807 between slope features and block dynamics during bouncing and rolling. Assessing
808 the results of an experimental investigation, Azzoni and de Freitas (1995) commented
809 that the dispersion is generally in the range of 10% to 20%, regardless of the length of
810 the slope and that steeper slopes present smaller dispersion. Agliardi and Crosta
811 (2003) calculated lateral dispersion to be up to 34%, via high-resolution numerical
812 models on natural rough and geometrically complex slopes.

813 Lateral dispersion cannot be defined from the actual rockfall event in Ponti since only
814 one path is available. Using the simulated trajectories from RockyFor3D, which are in
815 the 3d space (Figure 4615), a lateral dispersion of approximately 60% is shown in the
816 middle of the distance between detachment point and the house. This is significantly
817 higher compared to the findings of Azzoni and de Freitas (1995) and Agliardi and
818 Crosta (2003). Moreover, based on the actual event and intuition, the lateral dispersion

819 computed by RockyFor3D is extremely pronounced ~~and most probably likely due to~~
820 ~~the topography effect of the area of detachment.~~ Specifically the origin of the rock
821 block is located practically on the ridgeline, facilitating the deviation of the rock fall
822 trajectory from the slope line. Examining Figure ~~46~~15, it is notable that the rock paths
823 are severely affected by ~~the topography factors.~~—Therefore, assessing lateral
824 dispersion seems to be a case specific task.

825 Asteriou & Tsiambaos (2016) defined deviation (e) as the dihedral angle between the
826 pre- and post-impact planes that contain the trajectory. They found that deviation is
827 controlled by the direction difference $\Delta\phi$, the slope inclination and the shape of the
828 block. For a parallel impact (i.e. $\Delta\phi=0^0$) a spherical block presents significantly less
829 deviation compared to a cubical. Additionally, deviation is equally distributed along the
830 post-impact direction and reduces as the slope's inclination increases. On oblique
831 impacts the block's direction after impact changes towards the aspect of slope and as
832 $\Delta\phi$ increases this trend becomes more pronounced.

833 Figure ~~47~~16 presents deviation as a function of direction difference. It is noted that for
834 parallel impacts deviation is also equally distributed along the post-impact direction.
835 As direction difference increases, deviation becomes positive, which means that the
836 change of direction is following the direction of slope's aspect. These findings are in
837 line with trends described by Asteriou & Tsiambaos (2016), but the deviation of the
838 actual trajectory is significantly lower. This can be attributed to the different conditions
839 (i.e. block shape, slope material, slope roughness, incident velocity and angle, and
840 scale) between the experimental program conducted by Asteriou & Tsiambaos (2016)
841 and the Ponti rockfall event.

842 **7. Discussion - conclusions**

843 UAV-enabled reconnaissance was successfully used for the identification of the origin
844 of the detached rock, the rockfall trajectory and the impact points on the slope,
845 emphasizing on the motion types of the trajectory (rolling and bouncing sections). A

846 ~~drone-UAV~~ with an ultra-high definition (UHD) camera was deployed to reach the
847 inaccessible, steep and partly vegetated uphill terrain. A high-resolution orthophoto of
848 the rockfall trajectory and a 10 cm DSM was prepared, which formed the basis for an
849 analytical 2D kinematic analysis and a comparison with the outcomes of 2D and 3D
850 rockfall analysis software.

851 The initial velocity of the detached rock was estimated based on site conditions and
852 amplification of the ground acceleration due to topography. It was found that the
853 estimation of the initial velocity of the blocks plays a significant role in the accurate re-
854 production of the rockfall trajectory.

855 Based on the analytical analysis performed, it was found that the coefficients of
856 restitution cannot be directly connected to the material type, nor can be considered ~~as~~
857 constants. The impact angle seems to pose a consistent effect on normal COR, which
858 has been observed~~seen~~ also in other recent relevant studies, but has not been
859 incorporated yet on analyse~~s~~ models.

860 It was proven impossible to replicate the actual trajectory of the rock fall by
861 ~~p~~Performing a 2D rockfall analysis with the set of parameters recommended by the
862 developers, ~~was impossible to replicate the actual trajectory~~ revealing some limitations
863 in the present formulations. In an attempt to match the actual rock path to the analysis
864 output, the friction angle of the limestone slope was considered equal to zero.
865 However, the falling rock still rolled on the slope and stopped much earlier than its
866 actual runout distance while the impacts on the ground in the bouncing section of the
867 trajectory were considerably different in number and in location compared to the actual
868 ones.

869 Using the 3D analysis software, some rock trajectories better approximated the actual
870 trajectory using the suggested values by the software developers, indicating~~testifying~~
871 that the 3D analysis can be more accurate than the 2D analysis.

872 Based on the aforementioned analyses it becomes evident that engineering judgement
873 and experience must accompany the usage of commercial rockfall software in order to
874 acquire realistic paths. One should never ~~blindly use~~rest on the suggested set of
875 parameters since ~~the actual outcome~~field performance can differ significantly, as
876 demonstrated by this case study.

877

878 **References**

- 879 1. Agliardi F, Crosta GB (2003) High resolution three-dimensional numerical
880 modelling of rockfalls. International Journal of Rock Mechanics and Mining
881 Sciences 40:455-471. doi: 10.1016/S1365-1609(03)00021-2
- 882 2. Asteriou P, Saroglou H, Tsiambaos G (2012). Geotechnical and kinematic
883 parameters affecting the coefficients of restitution for rock fall analysis.
884 International Journal of Rock Mechanics and Mining Sciences 54:103-113.
885 doi:10.1016/j.ijrmms.2012.05.029.
- 886 3. Asteriou P and Tsiambaos G. (2016). Empirical Model for Predicting Rockfall
887 Trajectory Direction. Rock Mechanics and Rock Engineering 49.3, pp. 927–
888 941.
- 889 4. Azzoni A, de Freitas MH (1995). Experimentally gained parameters, decisive
890 for rock fall analysis. Rock Mechanics and Rock Engineering 28:111-124. doi:
891 10.1007/BF01020064
- 892 5. Buzzi O, Giacomini A, Spadari M (2012) Laboratory investigation on high
893 values of restitution coefficients. Rock Mechanics and Rock Engineering 45:35-
894 43
- 895 6. Crosta GB, Agliardi F (2004) Parametric evaluation of 3D dispersion of rockfall
896 trajectories. Natural Hazards and Earth System Science 4:583-598.
897 doi:10.5194/nhess-4-583-2004

- 898 7. Descoedres F, Zimmermann TH. Three-dimensional dynamic calculation of
899 rockfalls. In: Proceedings of the 6th International Congress on Rock
900 Mechanics. Montreal; 30 August -3 September 1987. p. 337–42.
- 901 8. Dorren, L.K.A., 2012. Rockyfor3D (v5.1) revealed - Transparent description of
902 the complete 3D rockfall model. ecorisQ paper, 31 p.
- 903 9. Ganas, A., Briole, P., Papathanassiou, G., Bozionelos, G., Avallone, A.,
904 Melgar, D., Argyrakis, P., Valkaniotis, S., Mendonidis, E., Moshou, A. and Elias,
905 P. (2015). A preliminary report on the Nov 17, 2015 M=6.4 South Lefkada
906 earthquake, Ionian Sea, Greece, Report to EPPO, December 4 2015.
- 907 10. Ganas A., Elias P., Bozionelos G., Papathanassiou G., Avallone A.,
908 Papastergios P. Valkaniotis S., Parcharidis I., Briole P. (2016). Coseismic
909 deformation, field observations and seismic fault of the 17 November 2015 M
910 = 6.5, Lefkada Island, Greece earthquake. Tectonophysics 687, pp. 210–222.
- 911 11. Giani GP. Rock Slope Stability Analysis. Rotterdam: Balkema A.A; 1992.
- 912 12. Giacomini A, Thoeni K, Lambert C, Booth S, Sloan SW (2012) Experimental
913 study on rockfall drapery systems for open pit highwalls. International Journal
914 of Rock Mechanics and Mining Sciences 56:171-181.
915 doi:10.1016/j.ijrmms.2012.07.030
- 916 13. Ferrari F, Giani GP, Apuani T (2013) Why can rockfall normal restitution
917 coefficient be higher than one? Rendiconti Online Societa Geologica Italiana
918 24
- 919 14. Heidenreich B (2004) Small- and half-scale experimental studies of rockfall
920 impacts on sandy slopes. Dissertation, EPFL.
- 921 15. ITSAK (2016). Preliminary presentation of the main recording of ITSAK – OASP
922 accelerometer network in Central Ionian. Earthquake M6.4 17/11/2015.
923 Thessaloniki, 11 pp.

- 924 16. Karakostas, V. G., Papadimitriou, E. E., and Papazachos, C. B. 2004.
925 Properties of the 2003 Lefkada, Ionian Islands, Greece, Earthquake Seismic
926 Sequence and Seismicity Triggering. Bulletin of the Seismological Society of
927 America, 94 (5), 1976–1981, October 2004
- 928 17. Manousakis J., Zekkos D., Saroglou H., Clark M. (2016). Comparison of UAV-
929 enabled photogrammetry-based 3D point clouds and interpolated DSMs of
930 sloping terrain for rockfall hazard analysis. Proc. Int. Archives of the
931 Photogrammetry, Remote Sensing and Spatial Information Sciences, Vol. XLII-
932 2/W2, p. 71-78.
- 933 18. Marinos P, Tsiambaos G., 2002. Earthquake triggering rock falls affecting
934 historic monuments and a traditional settlement in Skyros Island, Greece. Proc.
935 of the Int. Symposium: Landslide risk mitigation and protection of cultural and
936 natural heritage, Kyoto, Japan, pp. 343-346.
- 937 19. Mavrouli O., Corominas J., Wartman J. (2009). Methodology to evaluate rock
938 slope stability under seismic conditions at Sol`a de Santa Coloma, Andorra.
939 Nat. Hazards Earth Syst. Sci., 9, 1763–1773. Micheletti N., Chandler J., Lane
940 S., 2015. Structure from Motion (SfM) Photogrammetry. British Society for
941 Geomorphology. *Geomorphological Techniques*, Chap. 2, Sec. 2.2 (2015)
- 942 21. Papathanassiou, G., Valkaniotis, S., Ganas, A. and Pavlides, S. 2012. GIS-
943 based statistical analysis of the spatial distribution of earthquake-induced
944 landslides in the island of Lefkada, Ionian Islands, Greece, Landslides, Journal
945 of the International Consortium on Landslides, DOI 10.1007/s10346-012-0357-
946 1
- 947 22. Papazachos B.C., Papadimitriou E.E., Kiratzi A.A., Papazachou C.B., Louvari
948 E.K. 1998. Fault plane solutions in the Aegean sea and the surrounding area
949 and their tectonic implication. Bull Geof Teor Appl 39(3), 199–218.

- 950 23. Paronuzzi P. (2009) Field Evidence and Kinematical Back-Analysis of Block
951 Rebounds: The Lavone Rockfall, Northern Italy. *Rock Mech Rock Eng*, 42:783–
952 813
- 953 24. Richards LR, Peng B, Bell DH (2001) Laboratory and field evaluation of the
954 normal Coefficient of Restitution for rocks. Proceedings of ISRM Regional
955 Symposium EUROCK2001:149-155
- 956 25. RocScience, 2004. Rocfall Manual.
- 957 26. Rondoyanni Th., Mettos A., Paschos P., Georgiou Ch. 2007. Neotectonic map
958 of Greece, scale 1:100.000, Lefkada sheet. I.G.M.E., Athens.
- 959 ~~26. Rondoyanni T, Sakellariou M, Baskoutas J, Christodoulou N (2012) Evaluation~~
960 ~~of active faulting and earthquake secondary effects in Lefkada Island, Ionian~~
961 ~~Sea, Greece: an overview. Nat Hazards 61(2), 843–860.~~
- 962 27. Saroglou, H. 2013. Rockfall hazard in Greece. Bulletin of the Geological
963 Society of Greece, vol. XLVII, no3, 1429-1438.
- 964 28. Saroglou, H., Marinos, V., Marinos, P., Tsiambaos, G. 2012. Rockfall hazard
965 and risk assessment: an example from a high promontory at the historical site
966 of Monemvasia, Greece. *Natural Hazards and Earth System Sciences*, 12,
967 1823–1836. doi:10.5194/nhess-12-1823-2012.
- 968 29. Snavely N., Seitz S.N., Szeliski R., 2008. Modeling the world from internet
969 photo collections. *International Journal of Computer Vision* 80: 189-210.
- 970 30. Spadari M, Giacomini A., Buzzi O., Fityus S., Giani G.P.(2011). In situ rockfall
971 testing in New South Wales, Australia. *Int J Rock Mech Mining Sci*, 49, pp. 84–
972 93.
- 973 31. Volkwein, A., Schellenberg, K., Labiouse, V., Agliardi, F., Berger, F., Bourrier,
974 F., Dorren, L. K. A., Gerber, W., and Jaboyedoff, M., 2011. Rockfall

975 characterisation and structural protection – a review, *Nat. Hazards Earth Syst.*
976 *Sci.*, 11, 2617–2651, doi:10.5194/nhess-11-2617-2011.

977 34. Westoby M.J., Brasington J., Glasser N.F., Hambrey M.J., Reynolds J.M.,
978 2012. ‘Structure-from-Motion’ photogrammetry: A low-cost, effective tool for
979 geoscience applications. *Geomorphology* 179 (2012) 300-314.

980 35. Wyllie, D. C. (2014). Calibration of rock fall modeling parameters.

981 International Journal of Rock Mechanics and Mining Sciences 67: 170-180

982 36. Zekkos D., Clark M., Cowell K., Medwedeff W., Manousakis J., Saroglou H.
983 Tsiambaos G. (2017). Satellite and UAV-enabled mapping of landslides caused
984 by the November 17th 2015 M_w 6.5 Lefkada earthquake. Proc. 19th Int.
985 Conference on Soil Mechanics and Geotechnical Engineering, Seoul 2017
986 (accepted for publication).

987

988

TABLES

989

Table 1. Accelerometer recordings

Component	Acceleration (cm/sec ²)	Velocity (cm/sec)	Displacement (cm)
NS-comp	363	59.3	21.27
EW-comp	327	34.1	14.01
Z-comp	256	17.7	6.56

990

991 Table 2. Impact points characteristics

Impact point	X (m)	Y (m)	app_dip (°)	$\Delta\phi$ (°)	e (°)
1	287.63	338	39.0	0	0
2	298.38	329.68	16.3	33	0
3	305.48	324.5	27.9	27	-1
4	321.54	314.83	41.0	11.6	0.5
5	365.34	287.6	30.4	11.9	0.3
6	373.32	284.85	39.7	10.6	1.8
7	425.1	261.64	14.7	6.6	-1.3
8	464.43	251.13	18.4	33.3	0.8
9	472.06	248.81	14.0	19.1	2.3
10	495.29	243.81	7.5	52.3	0.9
11	515.31	240.8	7.9	51	0.6
12	535.56	238.31	9.1	46.7	3
13	562.11	232.22	8.7	47.3	2.1
14	605.51	211.12	16.9	25.6	-1.7
15	619.1	204.48	27.1	4.6	-3
16	639.13	196.96	21.2	8	4.7
17	662.41	184	23.3	28.5	5.2
18	688.4	169.3	27.4	0.3	-2.5
19	712.23	157.67	25.4	0.5	0.1
20	745.28	143.16	21.9	0.5	-0.1
21	762.9	137.01	22.0	0.7	2
22	789.23	125.98	21.6	1.4	-0.8
23	801.53	132.75	8.4	0.2	0.1

992 Table 3. Parabolic paths characteristics for the minimum release velocity

Segment	$\Delta x(m)$	$\Delta y (m)$	$\theta_{cr} (^\circ)$	$V_{r,min}$	V_{impact}	a_i	V_{COR}	n_{COR}	t_{COR}
1-2	10.75	-8.33	26.8	7.19	13.19	44.5	0.55	0.71	0.31
2-3	7.1	-5.18	25.7	5.95	9.51	27.8	0.63	0.90	0.53
3-4	16.07	-9.66	31.5	9.45	12.68	9.6	0.75	3.86	0.38
4-5	43.79	-27.23	27.7	15.46	23.13	23.3	0.67	1.57	0.26
5-6	7.98	-2.75	35.7	7.47	10.49	14.9	0.71	2.52	0.30
6-7	51.78	-23.21	34.8	18.15	21.61	31.7	0.84	1.54	0.26
7-8	39.33	-10.5	35.9	17.23	24.01	36.1	0.72	0.94	0.56
8-9	7.63	-2.32	35.9	7.45	10.54	41.1	0.71	0.87	0.55
9-10	23.23	-5	40.5	13.58	13.12	30.7	1.03	1.65	0.70
10-11	20.02	-3.01	41.1	13.00	11.57	24.2	1.12	2.06	0.82
11-12	20.25	-2.49	40.9	13.26	11.22	17.6	1.18	2.94	0.82
12-13	26.55	-6.1	38.0	14.40	14.25	28.5	1.01	1.55	0.78
13-14	43.41	-21.1	32.9	16.33	25.70	40.9	0.64	0.64	0.63
14-15	13.59	-6.64	30.7	9.13	12.81	25.1	0.71	1.24	0.53
15-16	20.03	-7.52	33.8	11.67	15.42	29.8	0.76	1.33	0.42
16-17	23.27	-12.96	31.9	11.59	15.89	28.5	0.73	1.22	0.50
17-18	25.99	-14.7	29.9	12.20	20.11	30.9	0.61	0.95	0.42
18-19	23.83	-11.63	32.2	12.08	17.10	27.9	0.71	1.30	0.40
19-20	33.05	-14.51	33.6	14.55	20.62	32.1	0.71	1.14	0.43
20-21	17.62	-6.15	34.5	11.08	11.99	18.4	0.92	2.44	0.54
21-22	26.33	-11.03	35.1	13.11	16.33	27.3	0.80	1.47	0.49
22-23	12.3	6.77	58.1	14.30	13.97	48.9	1.02	1.34	0.28

993

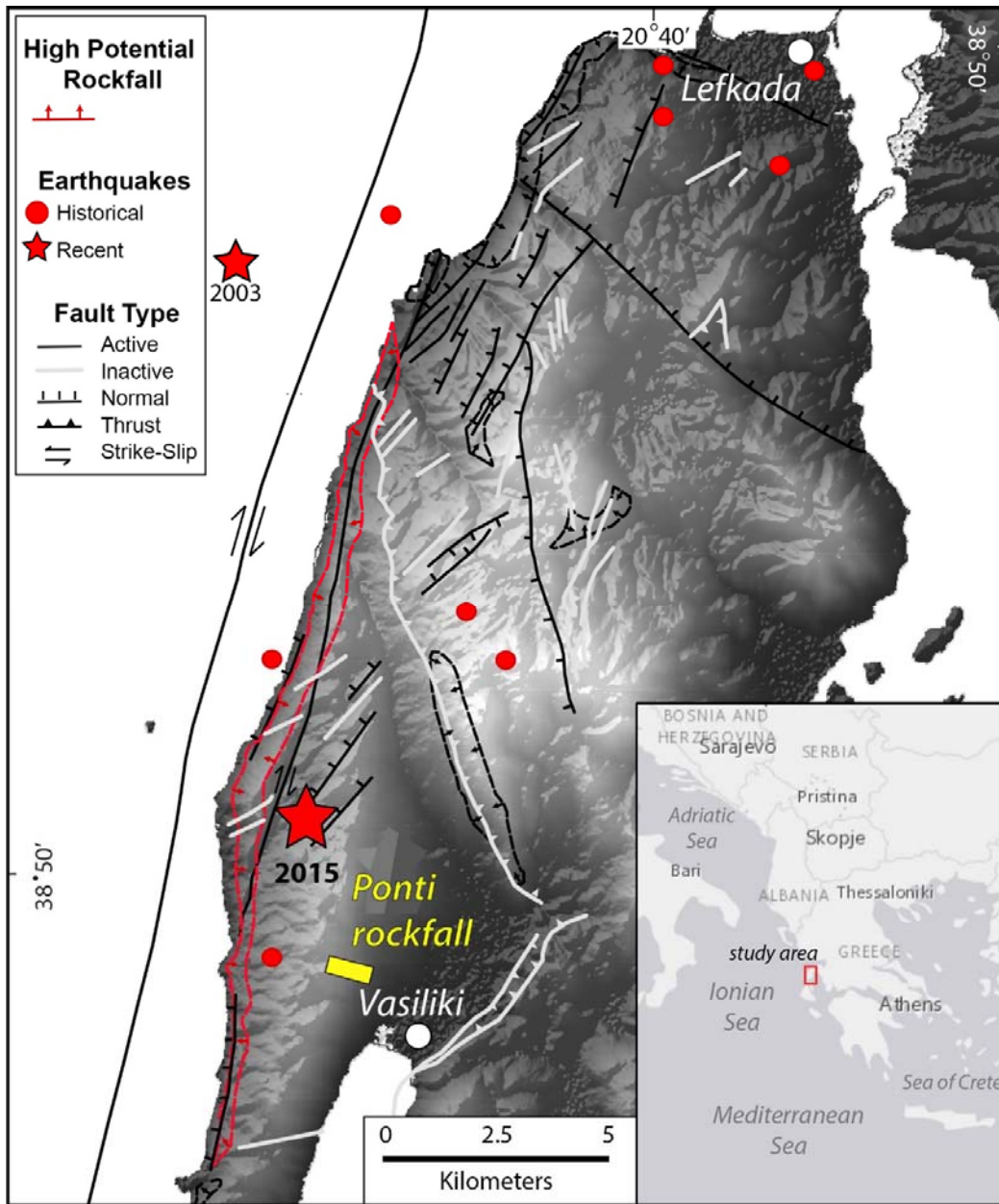
994

995 Table 4. Restitution parameters for Rockyfor3D

Geological formation/ other	Mean n_{COR}	MOH			Soil type (Rockyfor3D)
		rg70	rg20	rg10	
Scree ($\emptyset < \sim 10$ cm), or medium compact soil with small rock fragments	0.33	0.03	0.05	0.05	3
Talus slope ($\emptyset > \sim 10$ cm), or compact soil with large rock fragments	0.38	0.05	0.1	0.2	4
Talus with fallen boulders	0.42	0.15	0.15	0.2	4.1
Bedrock with thin weathered material	0.43	0	0.05	0.1	5
Asphalt road	0.35	0	0	0	7

996

FIGURES



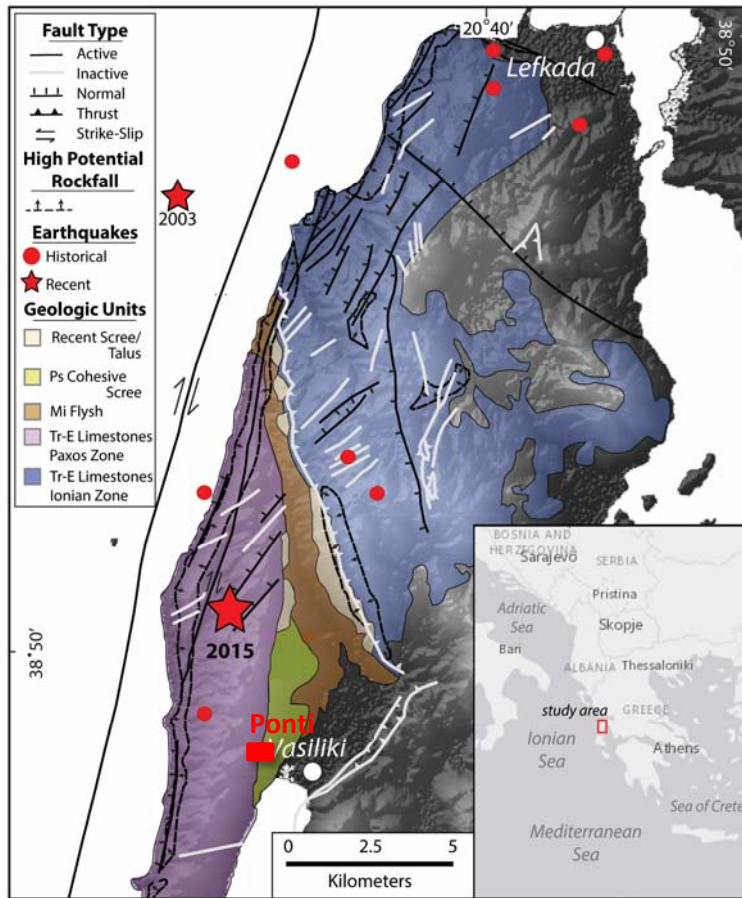


Figure 1. Neotectonic Map of Lefkada Island, Greece (Rondoyanni et al., 2012): with location of study site (Ponti) and epicenters of recent earthquakes (stars) in 2003 (M_w 6.2) and 2015 (M_w 6.5), as well as historical ones (circles) Map also shows faults and high potential rockfall areas as identified by Rondoyanni et al. (2007). -are shown-

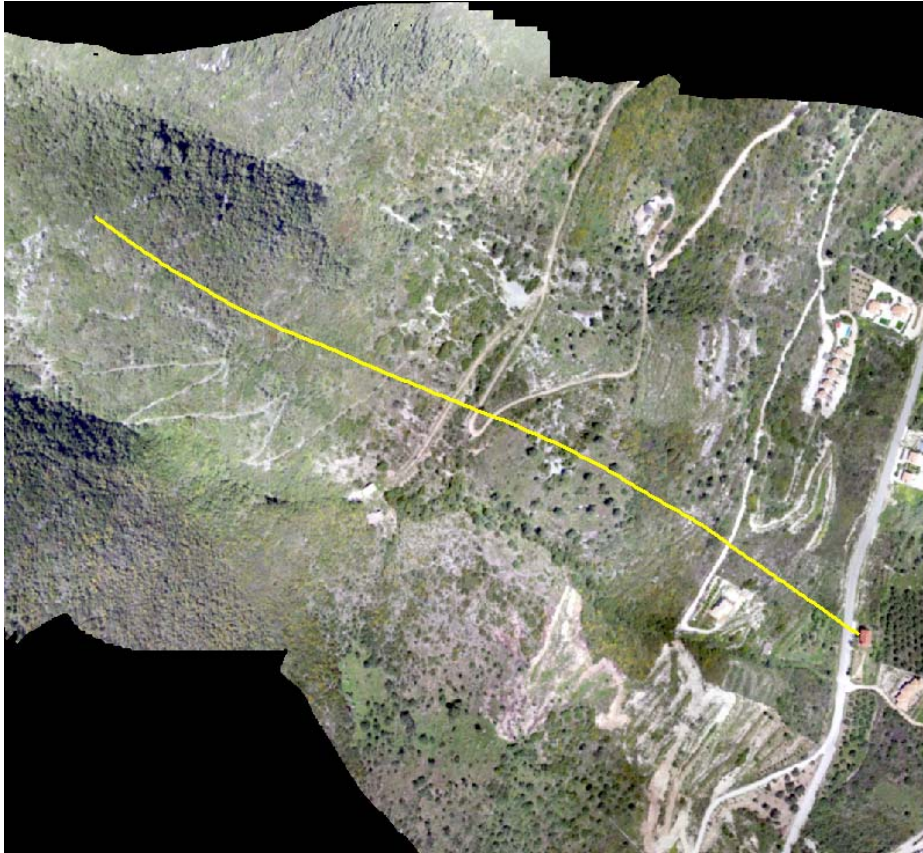


Figure 2. Orthophoto of study site, showing known trajectory and impact on house. The total length of the trajectory shown with a yellow line, is 800 m.



Figure 3. Impact of rock on house in Ponti, Lefkada, Greece.

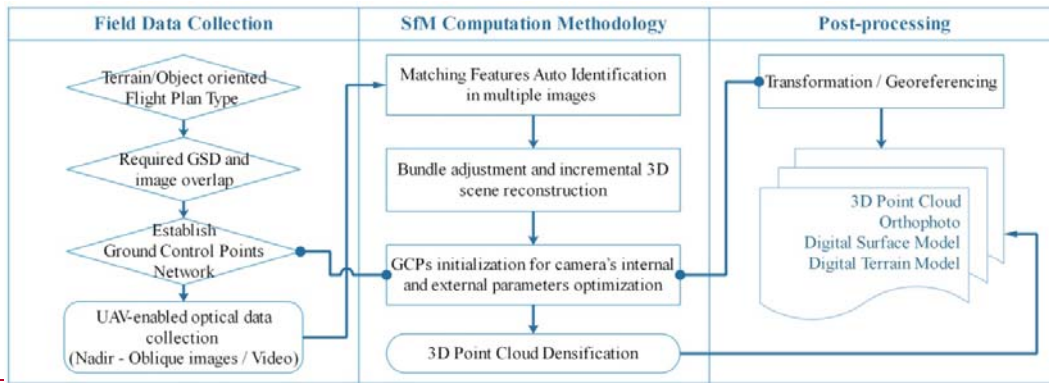


Figure 4. Workflow for Structure from Motion used in the present study.

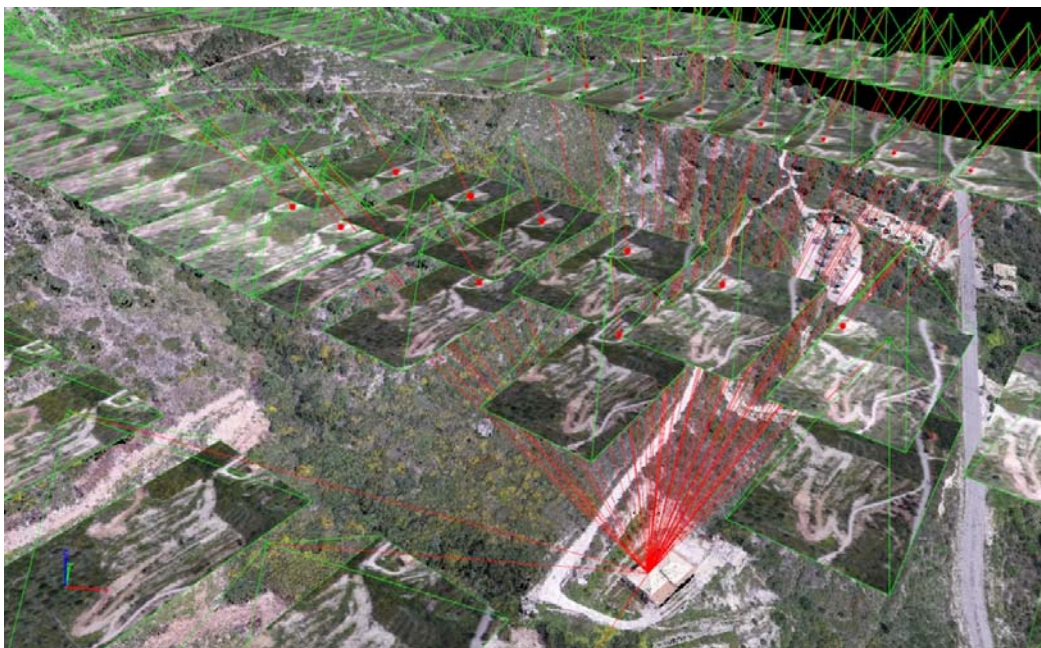


Figure 54. Schematic illustrating the overlap between pictures in the study site using SfM methodology.

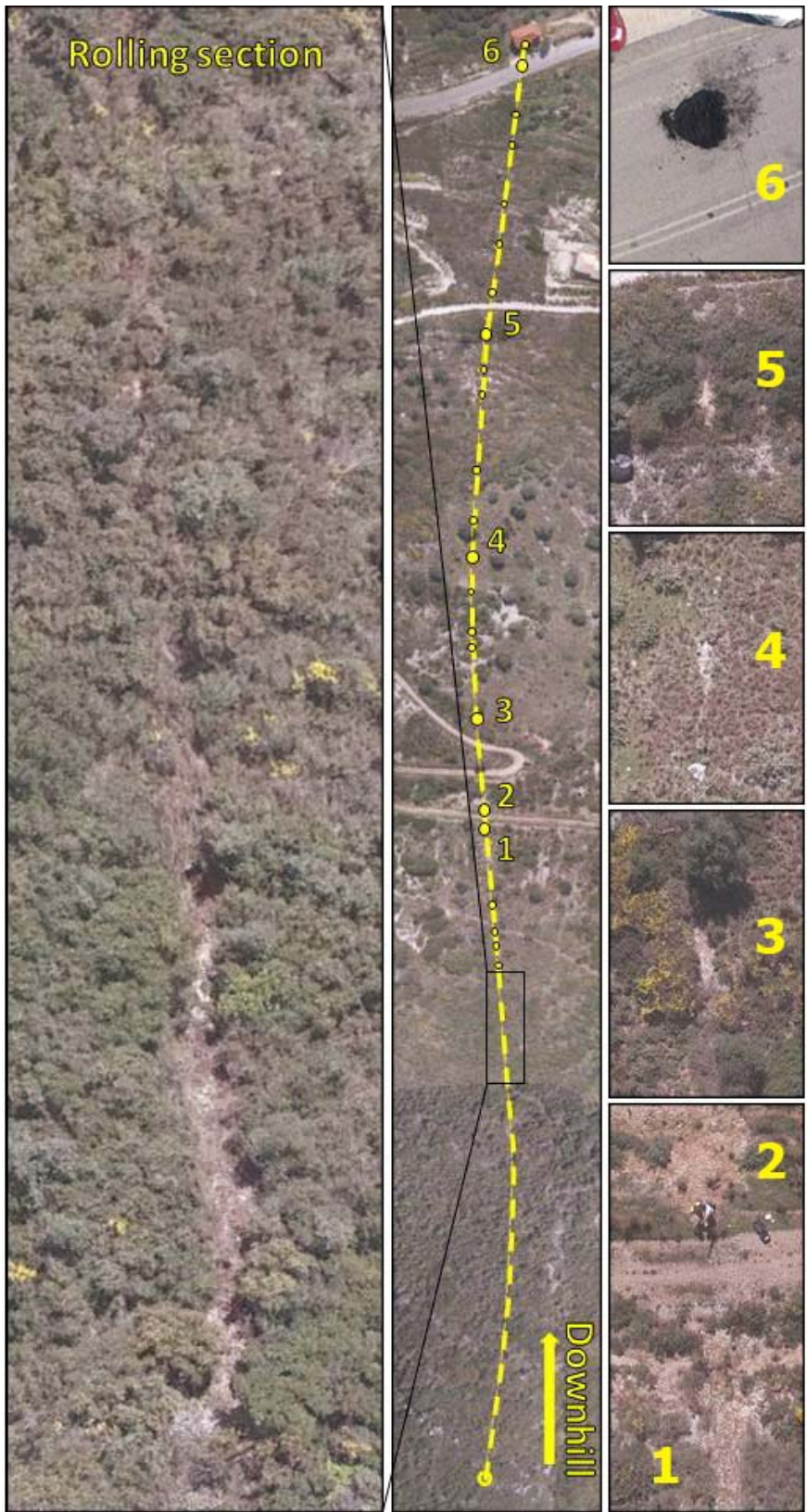


Figure 65. Top view orthophoto denoting rolling section, bouncing positions and indicative close-ups of impact points.

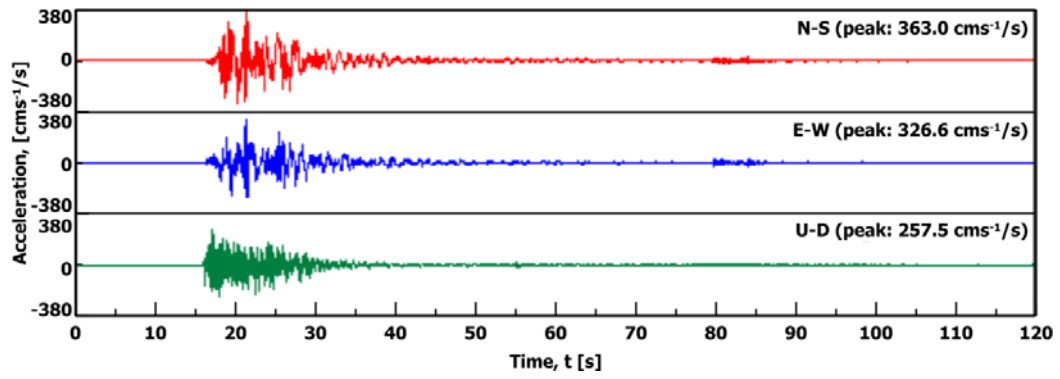


Figure 76. Acceleration recording at Vassiliki site (ITSAK, 2016)

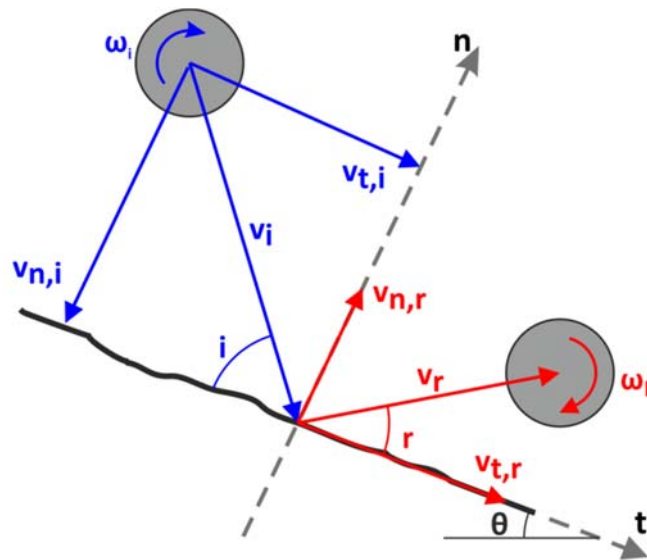


Figure 87. Coefficients of restitution

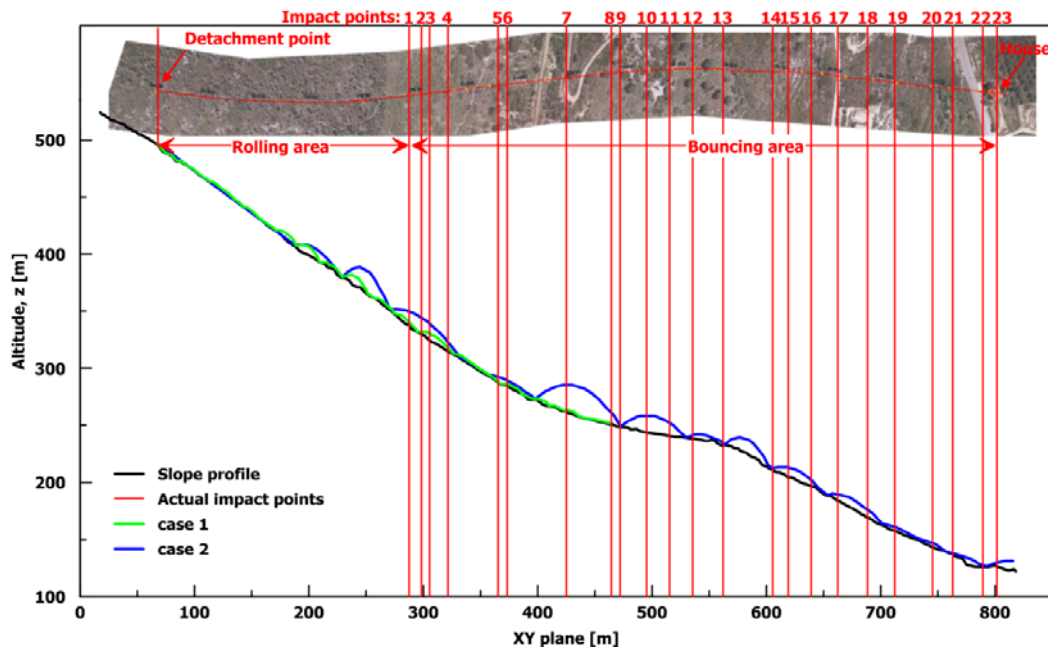


Figure 98. Plan view and cross section along block's path (units in m); 2D rockfall trajectory analysis results are plotted with green and blue line

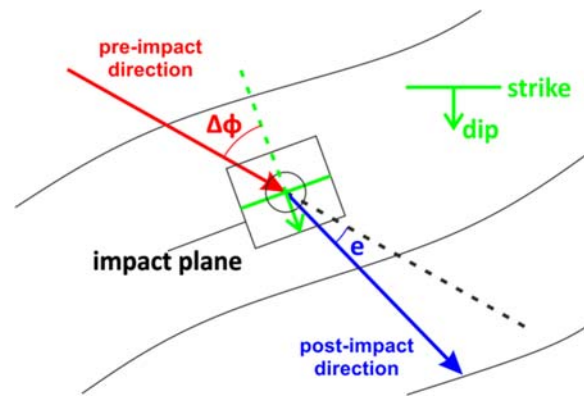


Figure 10-9: Out of plane geometry

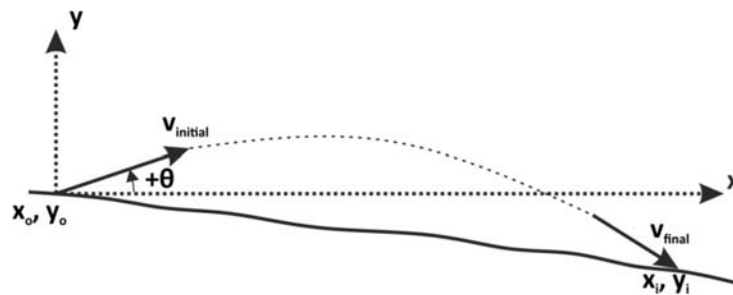


Figure 11-10. Parabolic segment

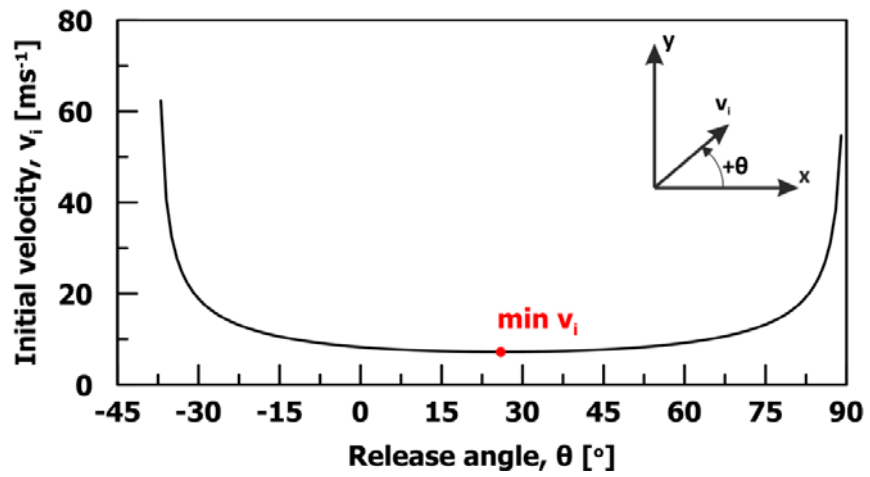


Figure 4211. Release angle versus initial velocity for the first parabolic section ($\delta x=10.75\text{m}$, $\delta y=8.33\text{m}$)

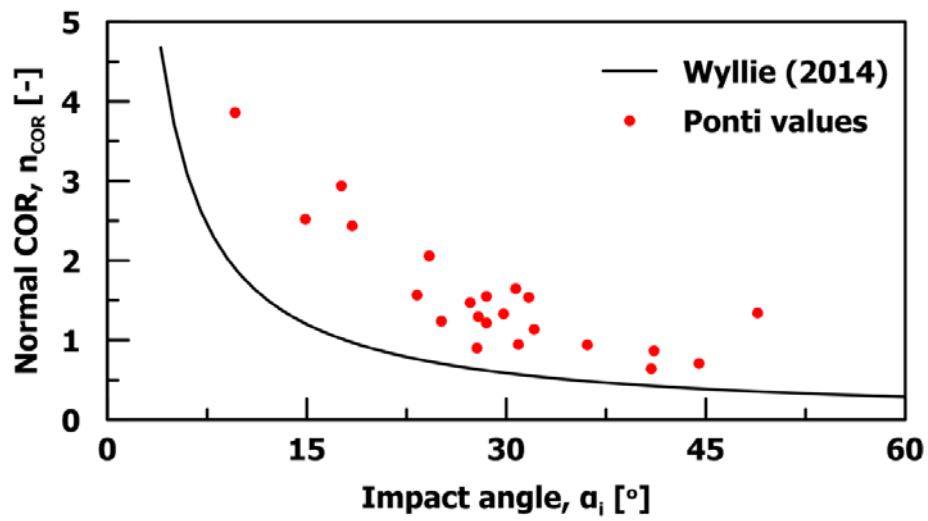


Figure 4312. Normal COR versus impact angle

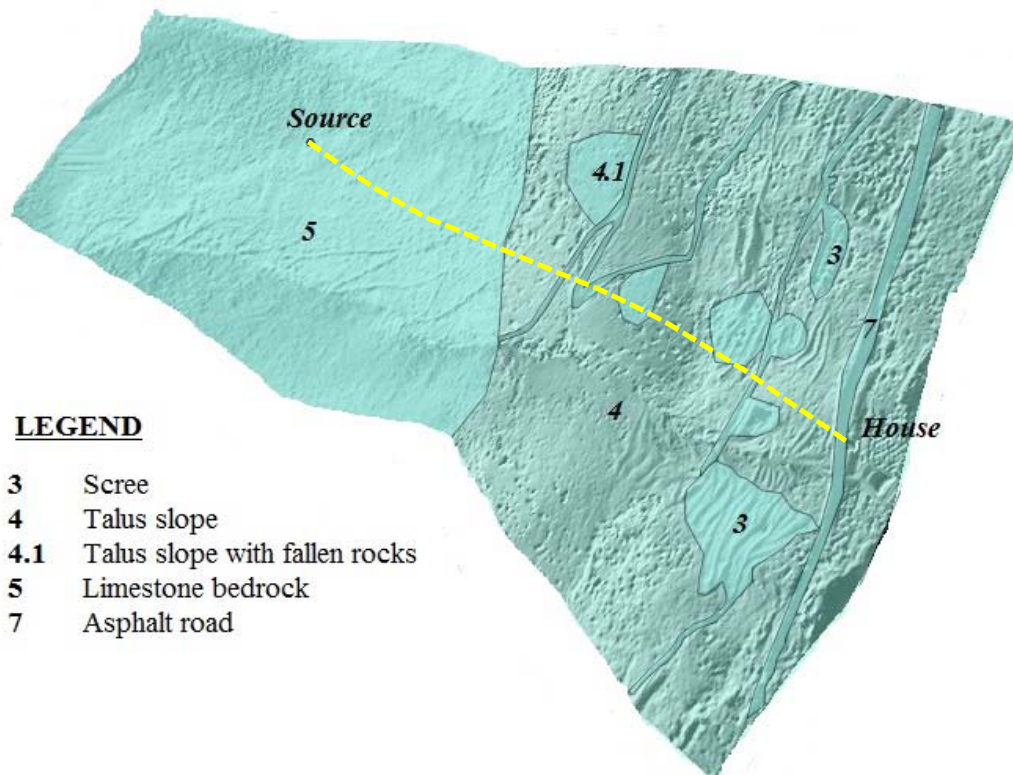


Figure 4413. Soil types for 3D rockfall analysis (according to Rockyfor3D). Yellow path of trajectory is 800 m.

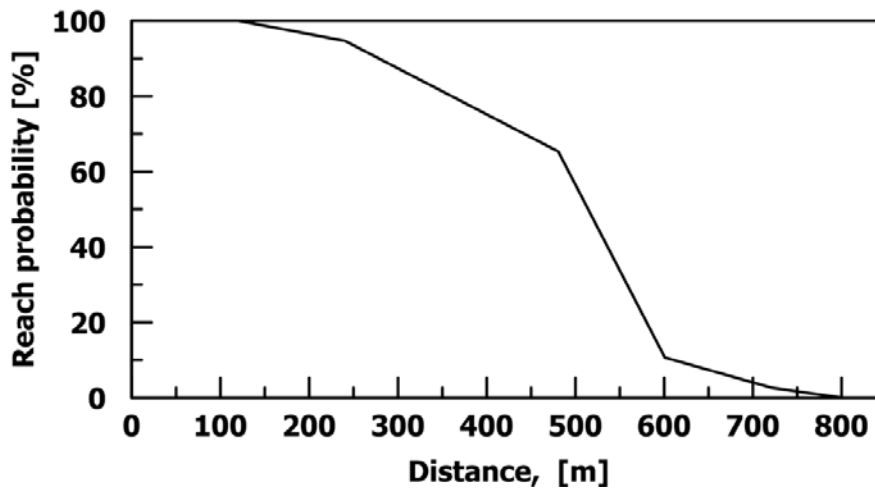


Figure 4514. Reach probability graph calculated from 3D rockfall analysis

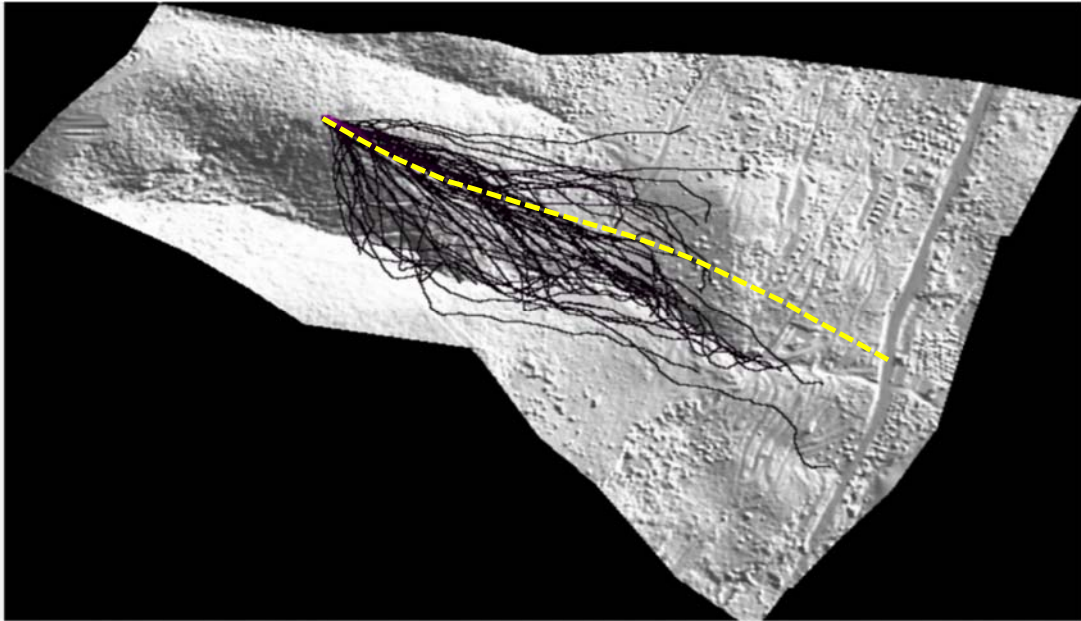


Figure 4615. 3D trajectory analysis (from RockyFor3D analysis). Yellow line shows the actual trajectory. Black lines show the simulated trajectory.

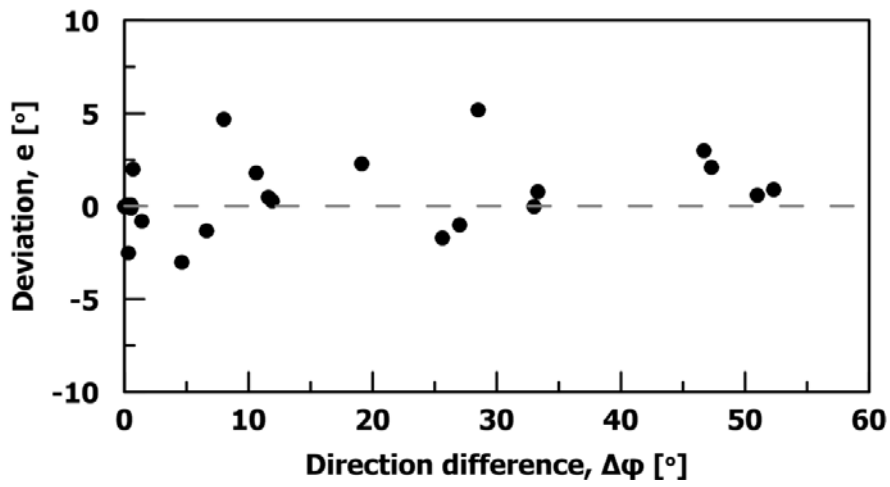


Figure 4716. Deviation as a function of direction difference.